buildings

MDPI

Article

Seismic Isolation Performance of Nuclear Power Plant Containment Structures

Zhicheng Xue [1,2,†], Xiujun Cui [3,4], Qiang Pei [3,†], Jintu Zhong [1,*], Yongyi He [1] and Yao Zhang [2]

[1] Architecture and Civil Engineering Institute, Guangdong University of Petrochemical Technology, Maoming 525000, China; xuezhicheng0630@163.com (Z.X.)
[2] College of Architecture and Engineering, Heilongjiang University of Science and Technology, Harbin 150020, China
[3] Key Laboratory for Prediction & Control on Complicated Structure System of the Education, Department of Liaoning Province, Dalian University, Dalian 116622, China; zjkjy1010@163.com (X.C.); peiqiang@dlu.edu.cn (Q.P.)
[4] School of Civil Engineering, Hebei University of Architecture, Zhangjiakou 075000, China
* Correspondence: zjt0339@163.com
† These authors contributed equally to this work.

Abstract: Non-isolated structures have strong destructive effects and poor isolation effects when encountering earthquakes. Setting isolation bearings can prolong the natural vibration period of the structure, reduce the horizontal seismic response of the structure under the influence of variables such as acceleration, base reaction, and inter story displacement, and enhance the overall seismic performance of the structure. The new material—epoxy plate thick layer rubber isolation bearing—has unique advantages compared to other bearings, such as effective energy absorption, simple construction, and low cost. This study establishes a three-dimensional isolated nuclear power plant containment structure based on the principle of similarity ratio, and compares and analyzes the acceleration, base reaction, and displacement responses of non-isolated and isolated structures. At the same time, the incremental dynamic analysis method (IDA) is used to analyze the seismic vulnerability of the structure, and the isolation performance of the nuclear containment structure using epoxy plate thick layer rubber isolation bearings is comprehensively and deeply explored. The results show that the epoxy plate thick layer rubber isolation bearing effectively prolongs the natural vibration period of the structure, reduces the horizontal seismic response of the structure, reduces the dome acceleration response by 66.55%, and reduces the base horizontal shear force by 55.51%. Therefore, setting epoxy plate thick layer rubber isolation bearings in the isolation layer can effectively enhance the seismic performance of the structure, thereby improving the redundancy of the nuclear power plant containment structure.

Keywords: epoxy plate thick layer rubber isolation bearing; time history analysis; seismic performance; incremental dynamic analysis method

Citation: Xue, Z.; Cui, X.; Pei, Q.; Zhong, J.; He, Y.; Zhang, Y. Seismic Isolation Performance of Nuclear Power Plant Containment Structures. *Buildings* **2024**, *14*, 1650. https://doi.org/10.3390/buildings14061650

Academic Editor: Marco Di Ludovico

Received: 22 April 2024
Revised: 20 May 2024
Accepted: 31 May 2024
Published: 3 June 2024

1. Introduction

Based on the development of basic isolation technology in nuclear power plants, relevant research has been conducted on the isolation design of nuclear power plant engineering structures in China. However, the isolation devices mainly use laminated rubber bearings and lead core rubber bearings, which can only achieve horizontal isolation of the structure. Due to the significant vertical seismic response of structures under strong earthquakes, three-dimensional isolation technology has become a hot research topic in nuclear power structural isolation. The safety shell structure of nuclear power plants serves as a protective barrier for nuclear reactors, and nuclear power engineering has high requirements for its seismic resistance. The application of three-dimensional isolation technology not only improves the safety of the safety shell structure of nuclear power

plants, but also shortens the construction period and reduces engineering costs. There is relatively little research on three-dimensional isolation technology for nuclear safety structures in China. The Institute of Engineering Mechanics of the China Earthquake Administration uses thick rubber isolation bearings to design the isolation of the safety shell structure. A systematic analysis of the seismic response of the safety shell structure under three-dimensional isolation was conducted using shaking table tests to verify the rationality of the isolation design. However, the performance and cost of the bearings deserve further research.

Isolation bearings are a widely used seismic technology in building structures, which can effectively reduce seismic loads and improve structural stability during earthquakes [1,2]. Isolation is mainly divided into rubber isolation and friction pendulum isolation. Rubber isolation bearings not only ensure the stability of the superstructure, but also effectively release stress. Park et al. studied the dynamic performance of lead rubber bearings and lead-free rubber bearings under seismic isolation, and found that the seismic performance of lead rubber bearings was better than that of lead-free rubber bearings. They also analyzed the dynamic response characteristics of lead rubber bearings under horizontal and vertical seismic motion [3]. Similarly, Jamalvandi et al. conducted a comparative study on lead rubber bearings and non-lead rubber bearings for storage tanks and found that lead rubber bearings have high isolation efficiency [4]. Lu et al. developed a simplified method for verifying the free vibration response of lead rubber bearings and linear natural rubber bearings in isolation design and seismic demand assessment, and obtained corresponding formulas [5]. Cao et al. proposed a lead rubber isolation bearing for multi-stage composite bridges that meets specific performance under different levels of seismic hazards to ensure isolation efficiency and limit the ability of bearings to move too much under different seismic effects. Research has shown that this bearing has high isolation efficiency for small- and medium-sized earthquakes and can effectively limit the displacement of the bridge [6]. In order to meet the application of isolation bearings in different structures and situations, researchers conducted a combination study on isolation bearings. Liu et al. prepared a hybrid isolation system that combines a buckling restrained brace (brb) with rubber bearings (RBs) or lead rubber bearings (LRBs) to meet all energy requirements under different seismic hazard levels, significantly improving the seismic performance of the bridge and reducing the seismic response under different earthquake scenarios [7]. Wang et al. The influence of rubber isolation bearings on the horizontal seismic resistance of nuclear power plants was studied through vibration table tests. Research has shown that rubber isolation bearings reduce horizontal acceleration and increase structural seismic margin [8]. Researchers conducted a series of shaking table tests to demonstrate that rubber isolation bearings have excellent isolation effects [9–11]. Rubber bearings have disadvantages such as low damping and large horizontal structural displacement, which affect the normal operation of buildings. Therefore, the emergence of friction pendulum sliding bearings has achieved more perfect earthquake control. Chen et al. conducted research on the seismic performance of bridges using an isolation scheme combining friction pendulum bearings and friction pendulum bearings with viscous dampers. The results showed that both friction pendulum bearings (FPB) and shock absorption and isolation combinations (CSDI) have good seismic absorption and isolation effects [12–14]. The above isolation bearings mainly focus on unidirectional isolation research. Although they can reduce the dynamic response of the structure to a certain extent, they ignore the synchronous isolation of horizontal and vertical directions. The development of three-dimensional bearings has broken through the limitations of unidirectional isolation [15]. Italy conducted relevant analysis on isolated nuclear reactor buildings. Frano et al. used the finite element method to numerically evaluate the dynamic response of the structure and establish a representative NPP structure three-dimensional model as accurately as possible, verifying the effectiveness of the isolation system [16]. Sun Feng et al. and Zhao Chunfeng et al. established a three-dimensional finite element model for the safety shell structure of nuclear power plants and further verified the effectiveness of isolation technology

through the time history analysis results of the structure [17–19]. Fan Shikai and Tan Pingping studied the CPR1000 reactor building of a nuclear power plant and established a mixed analysis model of the plant using concentrated particle beam elements and three-dimensional solid elements [20,21]. Md Ashiquzzaman et al. proposed the significant impact of soil structure interaction (SSI) on the isolation containment of nuclear power plants (NPPs) during very strong ground motion processes and represent the complete system of nuclear power plant containment building using a simplified model to express the impact of soil structure interaction on the nuclear power plant containment building [22]. Zhao Z et al. constructed a novel negative stiffness amplification system to enhance the isolation system (NSAS-IS). Due to the equivalent negative stiffness effect, installing NSAS-IS at the bottom of the containment structure can improve isolation, reduce the total energy dissipation burden of the main structure, and steadily dissipate strong vibration energy during multi intensity excitation, significantly improving the seismic performance of the containment structure [23]. Han G et al. studied the effect of ETLCDI on FPS isolation frames and conducted numerical analysis on a dual degree of freedom FPS isolation frame structure equipped with the optimal ETLCDI. Research has found that optimized ETLCDI can effectively handle the upper structure and bottom plate responses in severe earthquake events [24]. Through the isolation design of nuclear power isolation structures, the dynamic response before and after isolation was studied, the floor response spectrum of the equipment layer was analyzed, and the accuracy of the mixed analysis model and the effectiveness of isolation technology for energy dissipation and seismic reduction were verified. Wei Lushun, Zhang Yongshan, and others designed a separated three-dimensional isolation control system and conducted vibration table tests on a two-story steel frame structure using the system. This system combines base isolation technology with a vertical control system to reduce structural seismic response while controlling structural sway, providing reference for the seismic design of nuclear power engineering structures [25]. Nie et al. found through a series of shaking table tests and mechanical performance studies that three-dimensional isolation bearings have significant isolation effects in both horizontal and vertical isolation, laying the foundation for the actual function of isolation bearings and structural seismic design [26,27]. Zhuang et al. studied the mechanical performance of a separated three-dimensional isolation system through concept validation, and the results showed that the support effectively protected the structure from the influence of three-dimensional earthquakes and enhanced its load-bearing capacity [28]. Li and Zhang et al. studied the dynamic characteristics of three-dimensional bearings and found that they have good isolation and vibration reduction effects on three-dimensional isolation [29–31]. De Domenico D et al. investigated the hysteresis characteristics of an unbonded fiber-reinforced elastic isolator (UFREI) and determined the special effect attributed to the lateral coupling of the device through comparison with unidirectional test results. An effective nonlinear phenomenological model has been proposed to simulate the isotropic coupled biaxial hysteresis behavior of UFREI detected in experiments. The results indicate that by using non coupled models calibrated in unidirectional experiments, isolator displacement and upper structure acceleration are often higher, while ignoring bidirectional interactions [32]. Masato Abe et al. proposed a mathematical model for laminated rubber bearings under multi axial loads. The elastic-plastic model has been extended based on the one-dimensional model of bearings. And considering biaxial simple shear deformation simplifying the 3D constitutive relationship, a 2D elastic-plastic model was established. The ability of the proposed model to predict seismic response was verified, and triaxial mixed seismic response experiments were conducted. The results indicate that the model can accurately predict the response of experiments and improve seismic resistance [33].

In summary, from the research status of nuclear power isolation technology at home and abroad, although horizontal isolation bearings can achieve good isolation effects, they cannot effectively reduce the vertical vibration frequency and vertical seismic response of the structure. Although vertical isolation devices reduce seismic response and relative deformation, their energy dissipation capacity is average, which to some extent increases the

structural displacement response. The three-dimensional isolation bearings have significant isolation effects in both horizontal and vertical isolation. This article designs a new type of isolation bearing called "epoxy plate thick layer rubber isolation bearing" to study the seismic performance and seismic vulnerability of a special structure—nuclear power plant safety shell structures. This is to verify the superiority of 3D isolation and promote the application and promotion of 3D isolation technology in nuclear power engineering structures. Research has shown that the bearing not only has good three-dimensional seismic isolation effects, but also has a low material density, making it easy to transport and install. From the perspective of construction and environmental protection, it has expanded new directions for the field of seismic reduction and isolation in civil structures.

2. Introduction to Isolation Bearings

2.1. Design of Epoxy Thick Layer Rubber Isolation Bearings

By referring to the relevant specifications for bearing design, an orthogonal design method was used to optimize the design scheme and determine the main mechanical parameters of the horizontal stiffness, vertical stiffness, stability, and other mechanical properties of the epoxy thick layer rubber isolation bearing. The design process diagram of the epoxy thick layer rubber isolation bearing is shown in Figure 1. Based on these parameters, we determined the factors that affect the performance of the bearing, such as the diameter of the opening, the shear modulus of the rubber, and the thickness ratio of the rubber layer to the stiffener layer. Using the buckling stress, maximum shear stress, horizontal stiffness, and vertical stiffness of the support as control factors, we determined the optimal geometric dimensions and material parameters for the performance of epoxy thick layer rubber isolation bearings, as shown in Table 1. The design diagram of epoxy thick layer rubber isolation bearings is shown in Figure 2.

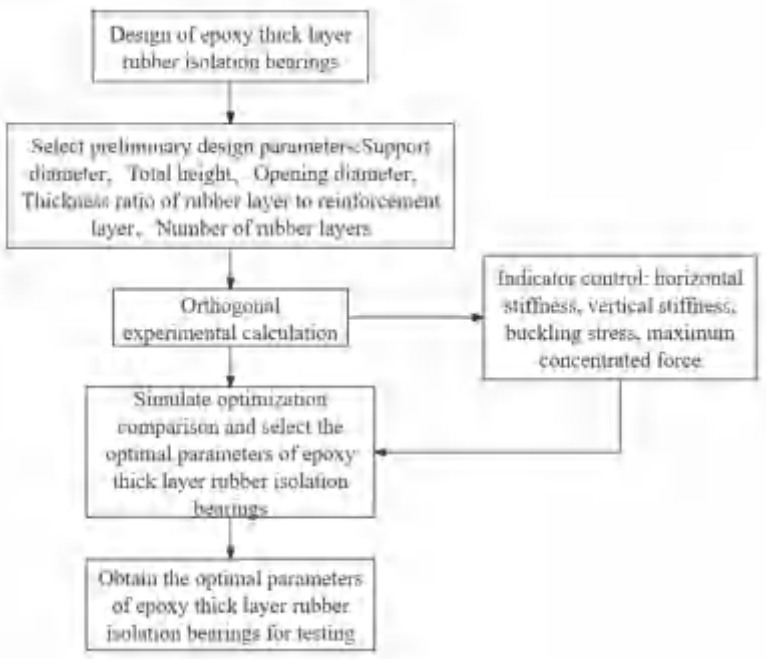

Figure 1. Design process diagram of epoxy thick layer rubber isolation bearings.

Table 1. Size table of epoxy resin board thick rubber isolation bearing.

Project		Parameter Value
Rubber	Shear modulus (G)/MPa	1.0
	Young's modulus (E_0)/MPa	5.1
	Bulk modulus (E_∞)/MPa	2160
	Rubber correction factor (k)	0.874
Rubber layer	Thickness (t_r)/mm	10.88
	Number (n)	9
	Total thickness (T_R)/mm	97.92
Internal epoxy resin board	Thickness (t_f)/mm	7.26
	Number ($n-1$)	8
	Total thickness (T_f)/mm	58.08
Design axial pressure/kN		300
Design stress/MPa		6.37
First shape coefficient (S_1)		5.74
Second shape coefficient (S_2)		2.55
Effective diameter of support (D)/mm		250
Opening diameter (D_0)/mm		0
Thickness of protective layer rubber (mm)		12
Thickness of upper and lower sealing plates (mm)		12
Thickness of connecting plate/mm		20
Total height of support		220
Horizontal stiffness/(kN/mm)		0.501
Vertical stiffness/(kN/mm)		99.125
Buckling stress/MPa		17.041

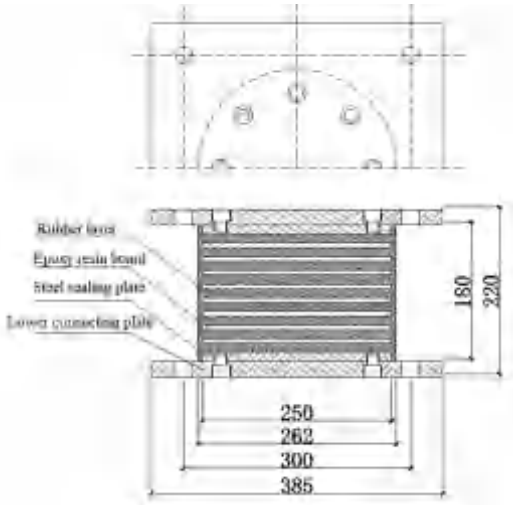

Figure 2. Design diagram of epoxy resin board thick rubber isolation bearing.

2.2. Selection of Isolation Units

The epoxy plate thick layer rubber isolation bearing has the same bearing restoring force model as the laminated rubber isolation bearing, as shown in Figure 3a. This model is an equivalent linear (linear elastic) model, with the main parameters being equivalent stiffness and equivalent viscous damping ratio [34]. Traditional models mainly consider the relevant parameters of horizontal isolation, while epoxy thick layer rubber isolation bearings have smaller vertical stiffness. Therefore, the support analysis model not only considers the horizontal stiffness and horizontal damping coefficient of the support, but also considers the vertical stiffness of the support. The structural isolation support model can be used to simulate the three-dimensional isolation of the structure by defining the

horizontal and vertical stiffness and damping of the support (as shown in Figure 3b). The damping coefficient C of the support is:

$$C = \frac{4\pi P\xi}{Tg} \quad (1)$$

where: P—vertical load borne by the isolation support, kN; T—The first natural vibration period of the isolated structure, s; ξ—Damping ratio; g—Gravitational acceleration, m/s^2.

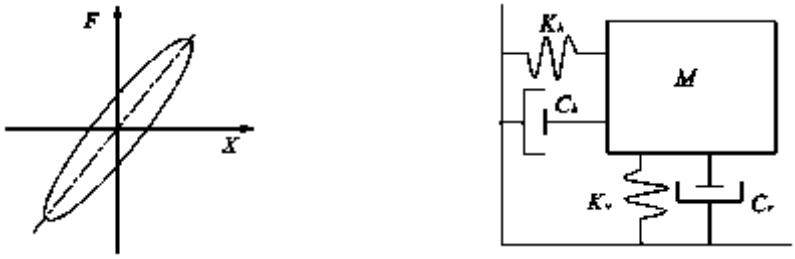

(**a**) (**b**)

Figure 3. Schematic diagram of the restoring force model and analysis model of rubber isolation bearings. (**a**) Equivalent linear type. (**b**) Isolation analysis model.

The simulation of rubber isolation bearings requires horizontal and vertical spring damping elements to constrain the rotation of both ends of the bearings, establish motion constraint relationships between different components through connectors, and then output variables for analysis. The simulation of the base isolation support establishes a translational relationship between two points through a Cartesian connector. The unit structure is shown in Figure 4, allowing for relative positional changes between point a and point b.

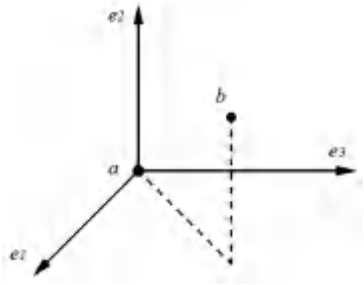

Figure 4. Cartesian connector.

For point a of the Cartesian connector, a local coordinate $\{e_1, e_2, e_3\}$ needs to be defined first. If the root uses the local coordinate system to determine the position and direction change of point b, then the position of point b relative to the point is defined as follows [35]:

$$x = e_1 \times (x_b - x_a);\ y = e_2 \times (x_b - x_a);\ z = e_3 \times (x_b - x_a)$$

Set the initial position of the point band and set the interaction force between point a and point b at that position to 0. Due to the selection of linear elastic analysis models for the support units, the three components of the Cartesian connector selected in the study are independent. The horizontal stiffness of the isolation support is set in the horizontal direction, and the vertical stiffness is set in the vertical direction. Its damping coefficient is added at the corresponding positions. Using a vertical pressure of 75 kN, the equivalent horizontal stiffness K_H = 0.56 kN/mm at 100% shear strain, damping ratio h_{eq} = 8.6%, and vertical stiffness K_V = 105 kN/mm.

3. Seismic Response Analysis of Nuclear Safety Shell Structures

3.1. Establishment of Finite Element Model for Containment Structure

3.1.1. Prototype of Containment Structure

The prototype structure of the containment vessel is a prestressed reinforced concrete containment vessel, with specific dimensions shown in Figure 5, where *R* represents the radius of the nuclear safety shell structure. The mass MP is 39,825 tons, and the material parameters of the cylinder concrete are: strength grade C40, elastic modulus E_p = 3.25 × 104 MPA, density ρ_P = 2400 kg/m^3. The geometric similarity ratio lr of the containment model is 1/15, and the material of the cylinder and dome is particulate concrete. The material parameter is M2.5 in strength; Elastic modulus: $E_m = 6.5 \times 10^4$ MPa; Density: ρ_P = 2300 kg/m^3; Poisson's ratio: μ = 0.2. The model steel bar material is galvanized steel wire, and the elastic modulus of the steel wire is $E_c = 2.1 \times 10^4$ MPa, Poisson's ratio of steel wire: μ = 0.25, mass density: ρ = 7800 kg/m^3.

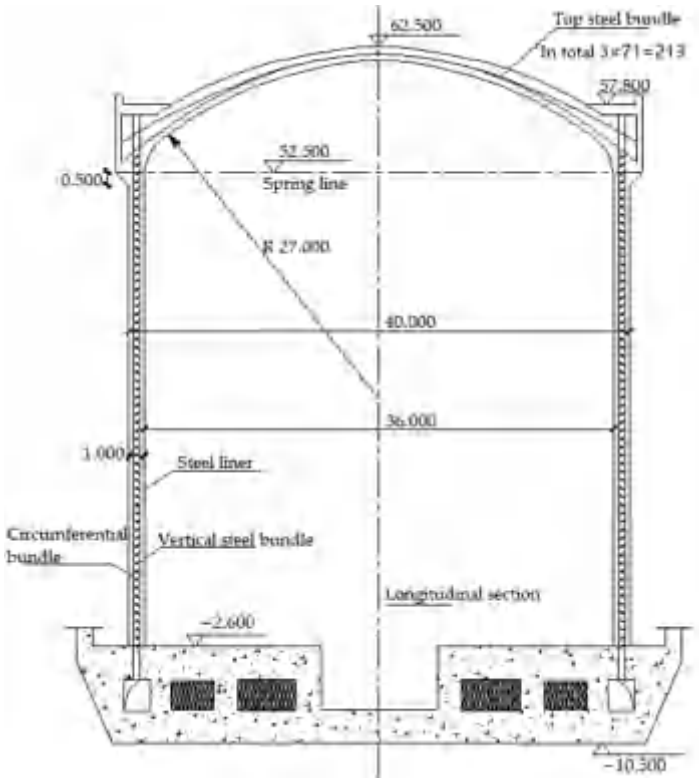

Figure 5. Geometric parameters of the containment structure of a nuclear power plant.

3.1.2. Similarity Relationship of Containment Structure Model

We established a safety shell structure under a mass model, taking the geometric similarity ratio, concrete elastic modulus similarity ratio, and concrete density similarity ratio as the basic parameters. We take the model weight of 6160 kg, and use similarity theory to derive the similarity ratios of other physical parameters [36–38]. The model similarity is shown in Table 2. The geometric size parameters of the containment test model obtained based on the similarity relationship are shown in Table 3. According to the actual reinforcement situation of the containment structure, galvanized iron wire is used to reinforce the dome and cylinder. The model section reinforcement diagram is shown in Figure 6. The test adopts a well-shaped beam base, and its plan is shown in Figure 7.

Table 2. Similarity ratio of the model.

Prototype Quality (kg)	M_p	39,825,000
Model quality (kg)	M_m	17,465
Gravity effect percentage		0.4934
Equivalent density		1.4802
Time	T_r	0.1814
Displacement	D_r	0.0667
Speed	V_r	0.3676
Acceleration	A_r	2.0268
Frequency	W_r	5.5138
Power	F_r	0.0009
Damping	C_r	0.0024
Stress	σ_r	0.2000

Table 3. Geometric parameters of the nuclear power plant containment structure model.

Model Parts	Size (m)	Model Parts	Size (m)
Inner diameter of the main cylinder wall	2.4	Dome thickness	0.05
Outer diameter of the main cylinder wall	2.52	Height from top plate to dome	4.625
Main cylinder wall thickness	0.06	Thickness of bottom cross beam	0.3
Height of main cylinder	3.675		

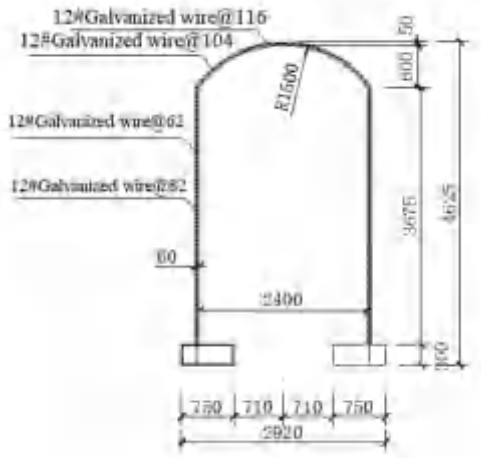

Figure 6. Model section reinforcement diagram.

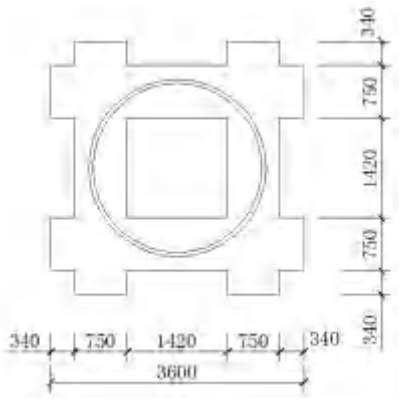

Figure 7. Base planar graph.

3.1.3. Analysis Model of Containment Structure

The finite element software ABAQUS was used to model the containment structure of a nuclear power plant. We set the stiffness and damping parameters of the three-dimensional isolation support in the isolation unit, and input the seismic motion through the loading platform. The seismic effect is transmitted to the Cartesian connector through the loading platform, and then to the upper structure. Using C3D8 and T3D2 elements for simulation, a three-dimensional discrete rigid body loading platform was established. Four isolation units were connected to the upper nuclear power plant containment structure test model, and a three-dimensional isolation nuclear power plant containment structure finite element model was established as shown in Figure 8.

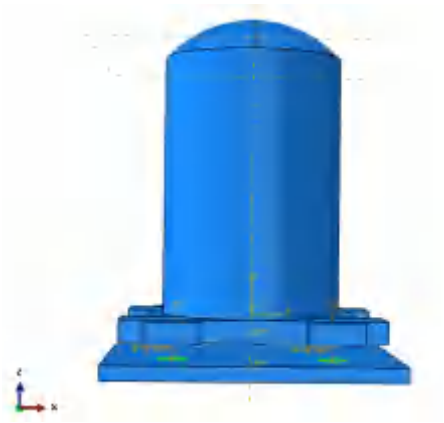

Figure 8. Finite element model.

3.2. Modal Analysis

Modal analysis is conducted on isolated and non-isolated containment structures, with the main analysis results including the natural frequency and mode of vibration of the structure, which are the inherent properties of the structure. Considering the torsional effect of the parallel torsional coupling calculation structure, the number of vibration modes should be calculated so that the participating mass of the vibration mode is not less than 90% of the total mass, and the number of vibration modes should not be less than 15. The Lanczos method was used to perform modal analysis on the three-dimensional finite element model of the safety shell structure of a nuclear power plant, and the natural frequencies and natural vibration periods of the non-isolated safety shell structure were obtained as shown in Table 4. The first two vibration modes of the non-isolated safety shell structure are mainly translational, while the third and fourth vibration modes form cylindrical ellipses at different angles, as shown in Figure 9. The finite element model of the safety shell structure of a three-dimensional isolated nuclear power plant was obtained through modal analysis, and its period and frequency are shown in Table 5. The first four vibration modes are shown in Figure 10. The period of the first main vibration mode of the safety shell structure of a non-isolated nuclear power plant is 0.34 s with a frequency of 29.53 Hz, and the vibration mode is mainly characterized by X-direction translational motion. Based on the comparison of structural modal results obtained from ABAQUS and SAP2000 [38], the structural period and frequency are very close (within the allowable error range) and the vibration mode remains consistent (as shown in Table 4), verifying the accuracy of the structural analysis model.

Table 4. Cycle and frequency of the various stages of the containment model.

Order	ABAQUS		SAP2000	
	Cycle (s)	Frequency (Hz)	Cycle (s)	Frequency (Hz)
1	0.0339	29.528	0.033	30.31
2	0.0338	29.529	0.033	30.31
3	0.0256	39.058	0.025	39.48
4	0.0256	39.056	0.025	39.48
5	0.0228	43.784	0.022	46.51
6	0.0228	43.815	0.022	46.51
7	0.0179	55.958	0.019	53.70
8	0.0179	55.987	0.019	53.70
9	0.0158	63.492	0.015	67.49
10	0.0135	74.081	0.013	77.54
11	0.0135	74.096	0.013	77.54
12	0.0133	75.148	0.013	78.97
13	0.0133	75.166	0.013	78.97
14	0.0118	84.718	0.012	80.41
15	0.0117	85.657	0.012	80.41

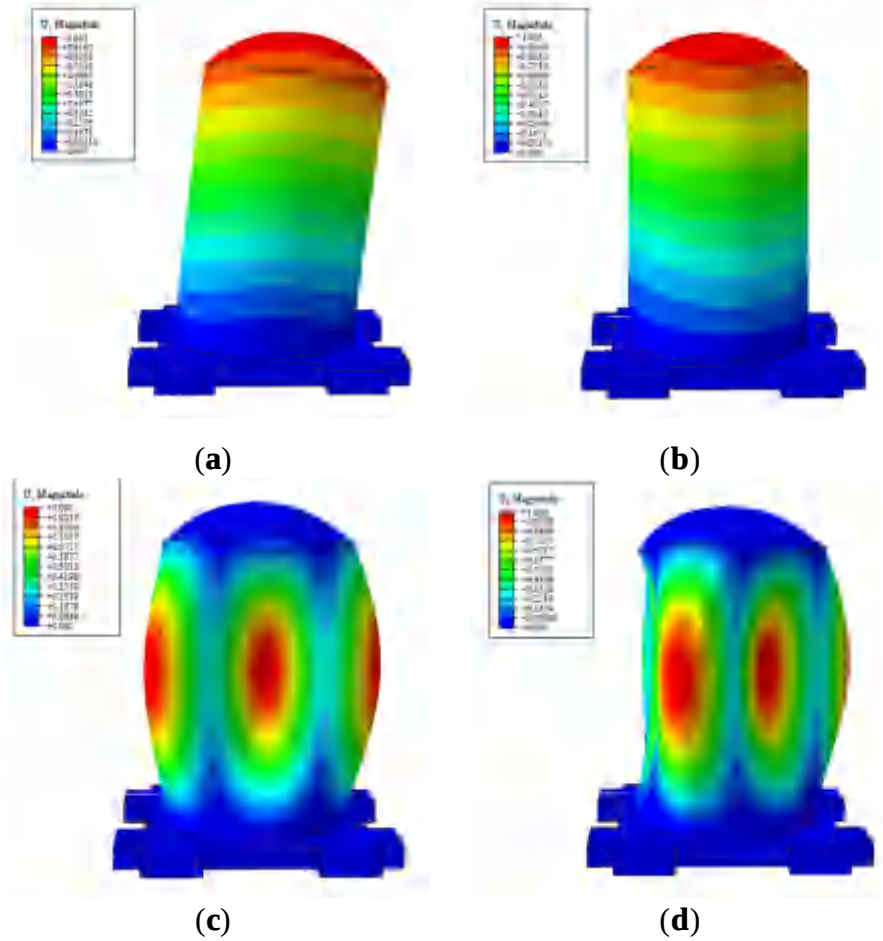

Figure 9. First to fourth vibration modes of non-isolated containment structures. (**a**) First vibration mode; (**b**) second vibration mode; (**c**) third order vibration mode; (**d**) fourth order vibration mode.

Table 5. Period and frequency of the first 15 modes.

Modal Order	Scale Model		Prototype	
	Frequency (Hz)	Cycle (s)	Frequency (Hz)	Cycle (s)
1	1.792	0.558	0.325	3.077
2	1.793	0.558	0.325	3.075
3	17.926	0.056	3.251	0.308
4	17.929	0.056	3.252	0.308
5	28.500	0.035	5.169	0.193
6	29.474	0.034	5.345	0.187
7	36.511	0.027	6.622	0.151
8	37.003	0.027	6.711	0.149
9	37.006	0.027	6.712	0.149
10	38.308	0.026	6.948	0.144
11	55.453	0.018	10.057	0.099
12	55.571	0.018	10.079	0.099
13	63.999	0.016	11.607	0.086
14	71.003	0.014	12.877	0.078
15	71.015	0.014	12.880	0.078

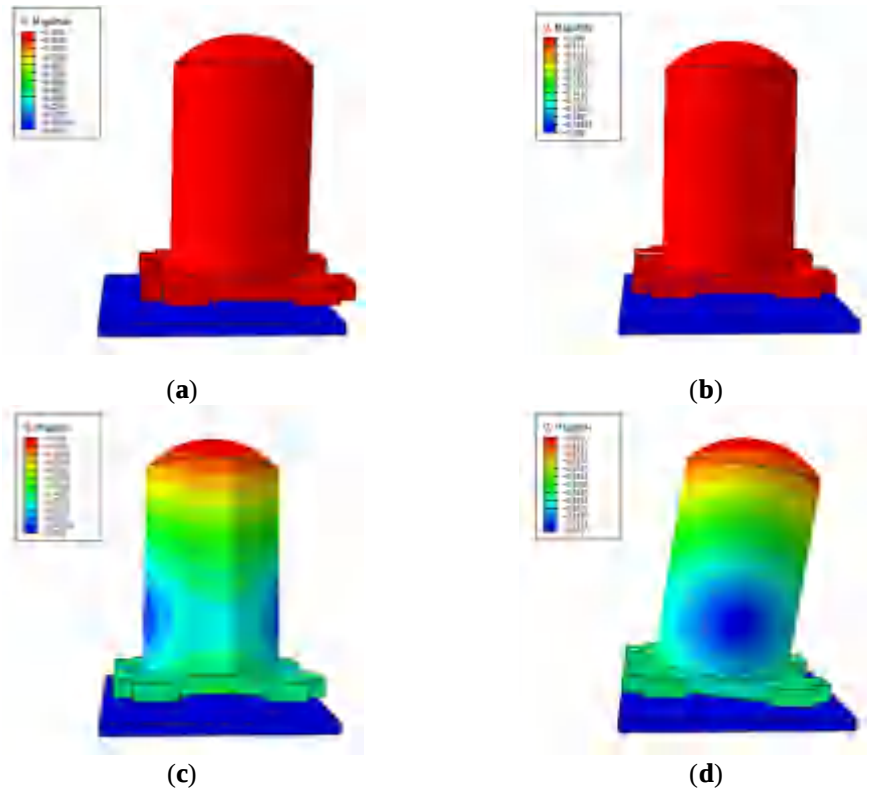

Figure 10. First to fourth order vibration modes of the safety shell structure model of a three-dimensional isolated nuclear power plant. (**a**) First vibration mode; (**b**) second vibration mode; (**c**) third order vibration mode; (**d**) fourth order vibration mode.

Compared to non-isolated nuclear power plant containment structures, the natural vibration period of three-dimensional isolation structures is longer. The natural vibration period of three-dimensional isolation structures is 0.558 s, and the theoretical calculation result is 0.555 s. The error between the two results is 0.5%, which verifies the accuracy of the model. According to the scale, the natural vibration period of the three-dimensional isolation structure of the nuclear power plant containment structure prototype is 3.077 s. From Figure 10, it can be seen that the first two vibration modes of the containment structure

of a three-dimensional isolated nuclear power plant are mainly translational, while the third and fourth vibration modes undergo torsion in the vertical direction.

3.3. Time History Analysis

(1) Damping determination

The dynamic analysis based on ABAQUS includes various damping models such as Rayleigh damping, direct modal damping, composite modal damping, and structural damping [39]. Rayleigh damping can describe the energy dissipation of structural systems. We compared the participation coefficients and effective mass of each vibration mode of the structure, and selected the first two vibration modes and their circular frequencies that play a dominant role in the structure ω_1 and ω_2. Then, we calculated the two parameters of Rayleigh damping α and β. Finally, we endowed the material with damping characteristics to simulate the true damping situation of the structure.

In Rayleigh damping, the viscous damping matrix can be expressed as:

$$[C] = \alpha[M] + \beta[K] \tag{2}$$

In the equation, α and β are calculated as follows:

$$\begin{Bmatrix} \alpha \\ \beta \end{Bmatrix} = \frac{2\omega_i\omega_j}{\omega_j^2 - \omega_i^2} \begin{bmatrix} \omega_j - \omega_i \\ \frac{-1}{\omega_j} \frac{1}{\omega_i} \end{bmatrix} \begin{Bmatrix} \xi_i \\ \xi_j \end{Bmatrix} \tag{3}$$

where ω_i, ω_j represents the i-th and j-th natural frequencies of the structure; and ξ_i, ξ_j represents the corresponding damping ratio.

Generally, $\xi_i = \xi_j = \xi$, and the damping ratio of reinforced concrete structures is generally $\xi = 0.05$. Based on the modal analysis results of nuclear power plant containment structures, $\omega_i = \omega_1 = 29.528$ Hz, and $\omega_j = \omega_2 = 29.529$ Hz are taken. After calculation, the Rayleigh damping coefficients $\alpha = 9.276$, $\beta = 0.00027$ are obtained.

(2) Ground motion selection and adjustment

When analyzing the elastic-plastic time history of the containment structure of a nuclear power plant, no less than two natural earthquake records and one artificial wave are selected as seismic inputs based on the site category and region where the structure is located, and the seismic grouping is designed [40]. Nuclear power plants belong to the Class A category of buildings and should be fortified by one degree [41]. Therefore, the seismic fortification intensity of the containment structure of nuclear power plants has been increased from 7 degrees to 8 degrees. As shown in Table 6, 0.3 g is taken as the basic seismic acceleration design. The site category is Class II, and the design earthquake group is Group III. According to Table 7, the characteristic period value of the site for the nuclear power plant containment structure is Tg = 0.45 s, with damping ξ = 0.05. Due to the uncertainty of seismic motion, considering that the spectral characteristics, effective peak value, and duration of seismic motion meet the specified requirements, the duration of strong earthquake records and artificial seismic motion should be 5–10 times the basic natural vibration period of the structure, and the duration of seismic motion should be taken as 30 s.

Table 6. The corresponding relationship between seismic fortification intensity and basic seismic acceleration.

Seismic Fortification Intensity	6 Degrees	7 Degrees	8 Degrees	9 Degrees
Design basic seismic acceleration (g)	0.05	0.10 (0.15)	0.20 (0.30)	0.40

Table 7. Characteristic period (s) [40].

Design Earthquake Grouping	Site Classification				
	I_0	I_1	II	III	IV
First set	0.20	0.25	0.35	0.45	0.65
Second set	0.25	0.30	0.40	0.55	0.75
Third set	0.30	0.35	0.45	0.65	0.90

Three seismic motions were selected for time-history analysis of the containment structure of a nuclear power plant, including EL-Centro waves, Taft waves, and one artificial wave. The seismic acceleration time-history curve is shown in Figure 11. The seismic motion is subjected to bidirectional loading using the acceleration time history, and based on the principle of similarity, its amplitude, duration, and step length are shown in Table 8.

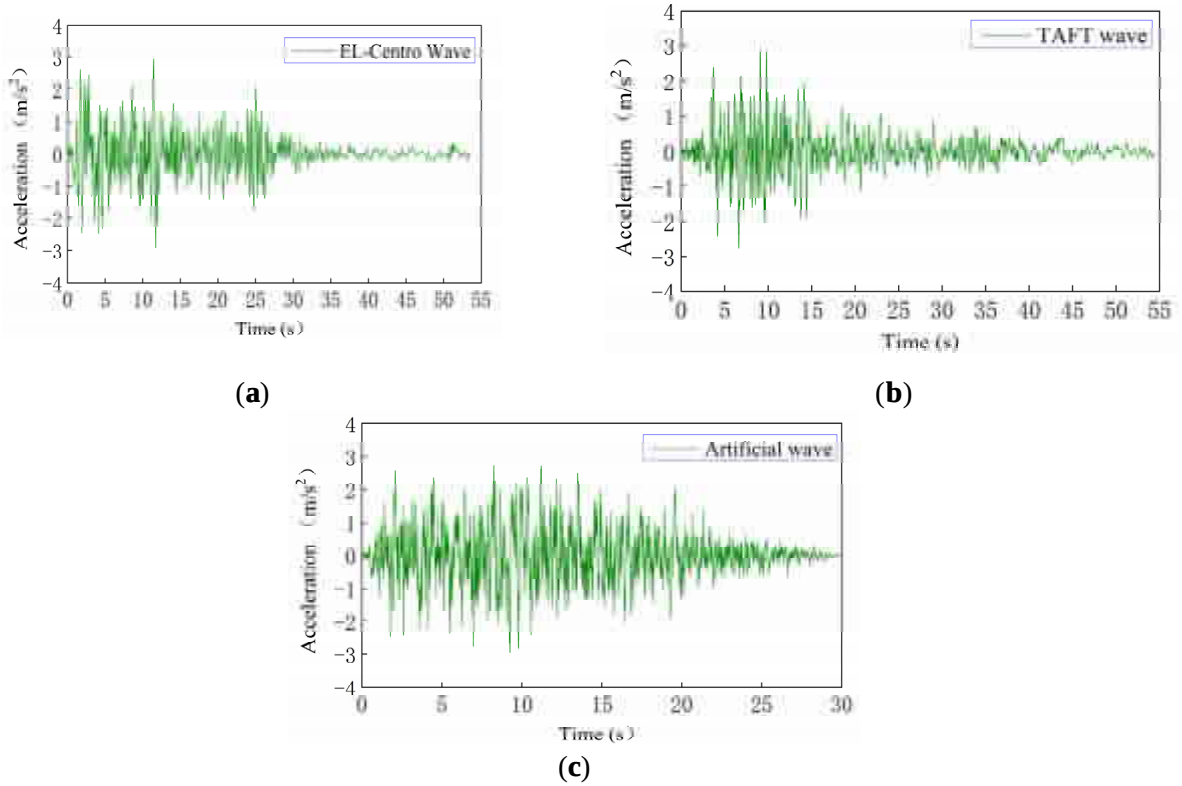

Figure 11. Earthquake ground motion acceleration time history. (**a**) EL-Centro wave; (**b**) Taft wave; (**c**) Artificial wave.

Table 8. Adjustment of earthquake ground motion amplitude, duration, and step size.

Direction	Prototype			Reduced Scale		
	Acceleration Amplitude (g)	Earthquake Duration (s)	Step (s)	Acceleration Amplitude (g)	Earthquake Duration (s)	Step (s)
X-direction	0.3	30	0.01/0.02	0.608	5.42	0.001814/0.003628
Z-direction	0.2	30	0.01/0.02	0.405	5.42	0.001814/0.003628

3.3.1. Structural Acceleration Response

(1) Acceleration response of non-isolated containment structures

The base acceleration and dome acceleration of the containment structure of nuclear power plants in the X and Z directions under different seismic motions are shown in

Figures 12–14. The maximum acceleration peak and amplification coefficient of the structural base and dome under different seismic motions are shown in Table 9.

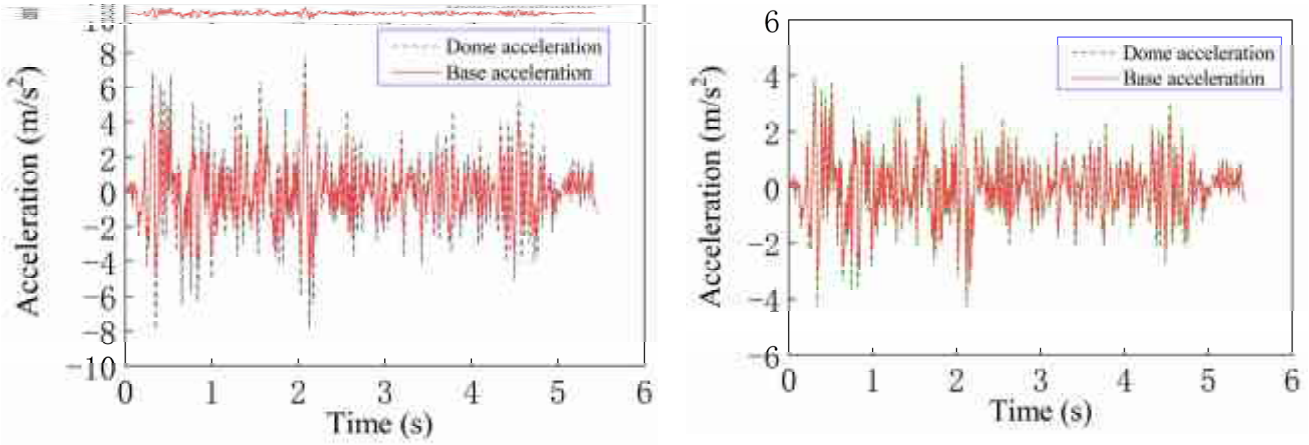

(**a**) (**b**)

Figure 12. Structural acceleration response under the EL-Centro wave. (**a**) X-direction acceleration response; (**b**) Z-direction acceleration response.

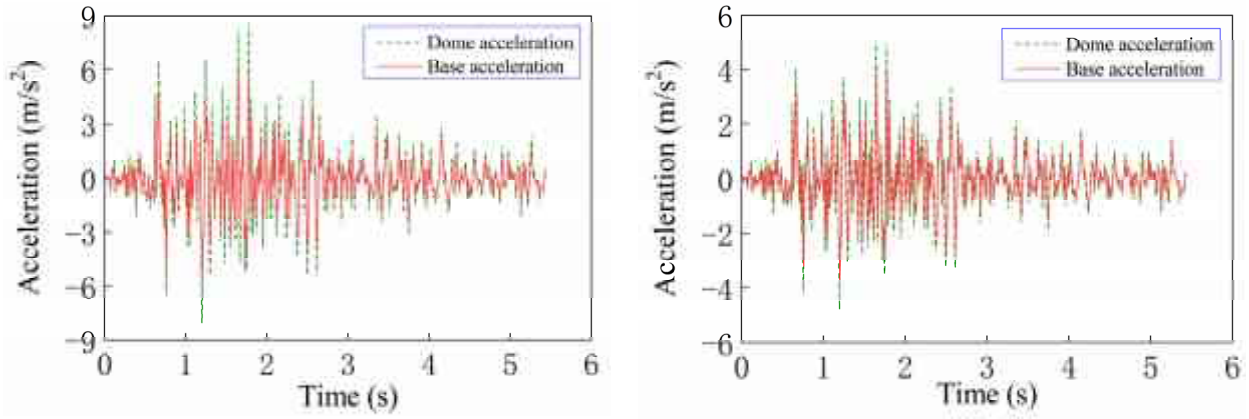

(**a**) (**b**)

Figure 13. Structural acceleration response under Taft wave. (**a**) X-direction acceleration response; (**b**) Z-direction acceleration response.

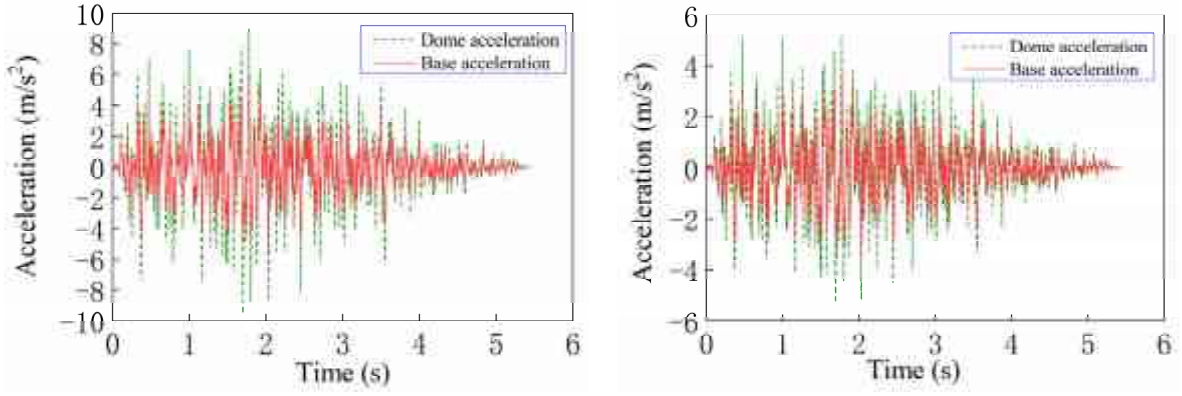

(**a**) (**b**)

Figure 14. Structural acceleration response under artificial wave. (**a**) X-direction acceleration response; (**b**) Z-direction acceleration response.

Table 9. Peak acceleration of the structural base and dome under different ground motions.

Type	Direction	Base Acceleration Peak (m/s^2)	Dome Acceleration Peak (m/s^2)	Amplification Factor
EL-Centro wave	X-direction	5.895	7.899	1.34
	Z-direction	3.923	4.433	1.13
Taft wave	X-direction	5.954	8.514	1.43
	Z-direction	3.966	4.958	1.25
Artificial wave	X-direction	5.834	9.568	1.64
	Z-direction	3.988	5.304	1.33

Under the action of seismic motion, the containment structure of a nuclear power plant has a certain amplification effect on seismic acceleration. Artificial waves have the highest amplification coefficient in the X and Z directions, while EL-Centro waves have the lowest amplification coefficient in the X and Z directions, mainly related to the characteristics of seismic motion. The seismic dominant frequency of artificial waves is relatively close to the natural frequency of the structure. The acceleration amplification coefficient of the nuclear power plant containment structure is between 1 and 1.7, with a small amplification coefficient. The base acceleration of the structure is consistent with the peak acceleration waveform of the structure, and there is almost no delay phenomenon, indicating that the structure has a large horizontal and vertical stiffness.

(2) Acceleration response of three-dimensional isolation structure

Under the action of the three seismic waves with an earthquake intensity of 0.608 g, the acceleration response values of the three-dimensional isolation nuclear power plant containment structure were analyzed and shown in Figures 15 and 16, and the amplification coefficients of the structural acceleration response were obtained as shown in Table 10.

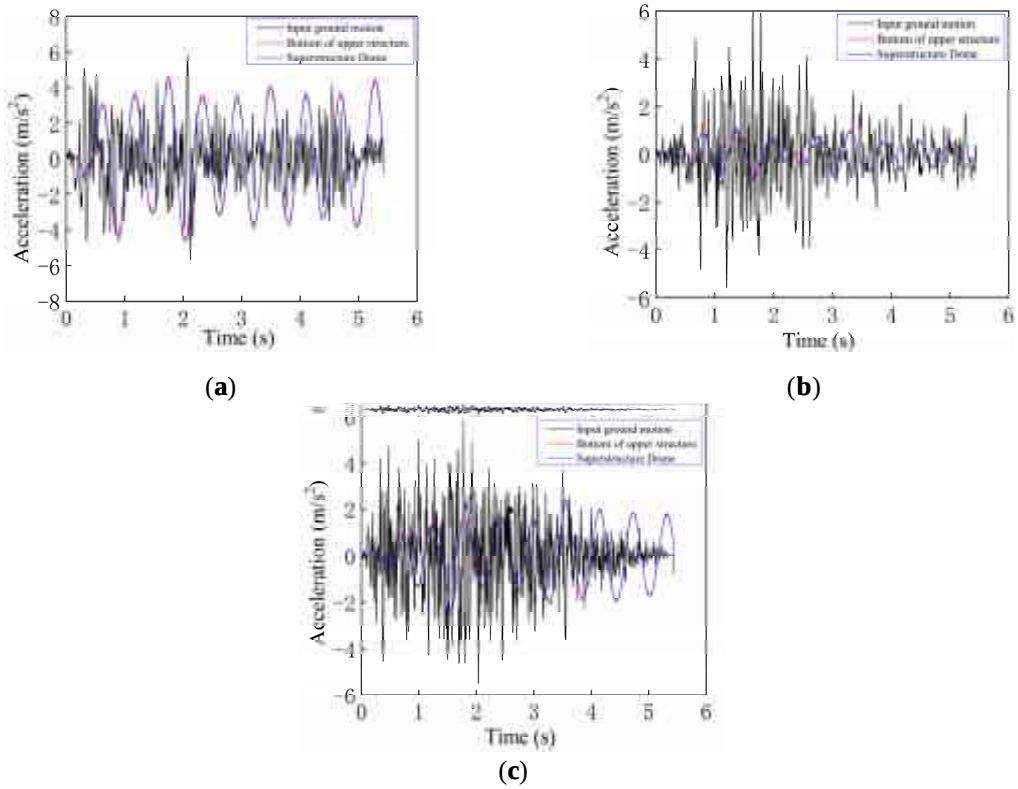

Figure 15. Acceleration response of the X-direction structure under different earthquake ground motions. (**a**) EL-Centro wave, (**b**) Taft wave, (**c**) Artificial wave.

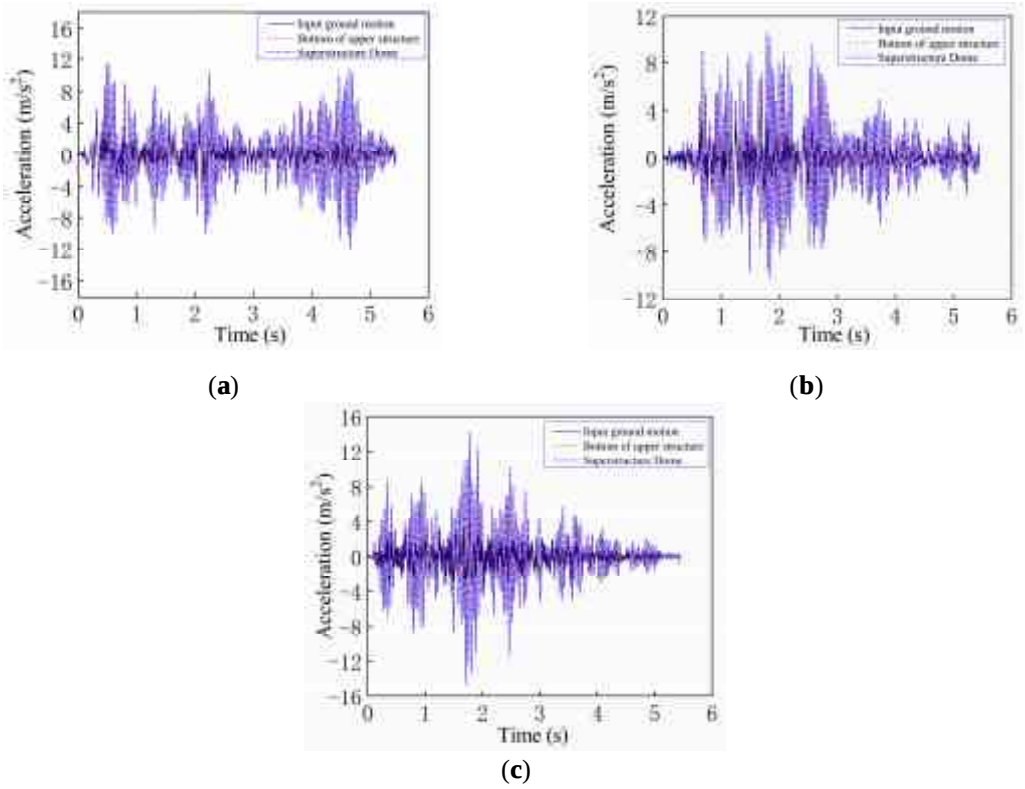

Figure 16. Acceleration response of the Z-direction structure under different earthquake ground motions. (**a**) EL-Centro wave, (**b**) Taft wave, (**c**) Artificial wave.

Table 10. Acceleration peaks of the structural base and dome under the action of various earthquake ground motions.

Type	Direction	Base Acceleration Peak (m/s^2)	Dome Acceleration Peak (m/s^2)	Amplification Factor
EL-Centro wave	X-direction	4.599	4.669	1.01
	Z-direction	11.523	12.135	1.05
Taft wave	X-direction	1.205	1.240	1.03
	Z-direction	10.035	10.788	1.08
Artificial wave	X-direction	2.341	2.556	1.09
	Z-direction	13.605	14.633	1.07

From Figures 15 and 16, it can be seen that under different seismic waves, the input seismic acceleration, upper structure bottom acceleration, and upper structure dome acceleration time history analysis curves of the three-dimensional isolation nuclear power plant containment structure in the X and Z directions are compared. The results indicate that compared to the input seismic acceleration, the acceleration response of the upper structure will be reduced and the amplitude of acceleration response reduction varies under different seismic actions.

3.3.2. Structural Base Reaction

(1) Non-isolated containment structure base reaction force

Under different seismic motions, the base reaction forces in different directions of the structure are shown in Figures 17–19. The magnitude of the reaction force is consistent with the acceleration waveform of the structure. The maximum base reaction force of the structure under different seismic motions is shown in Table 11.

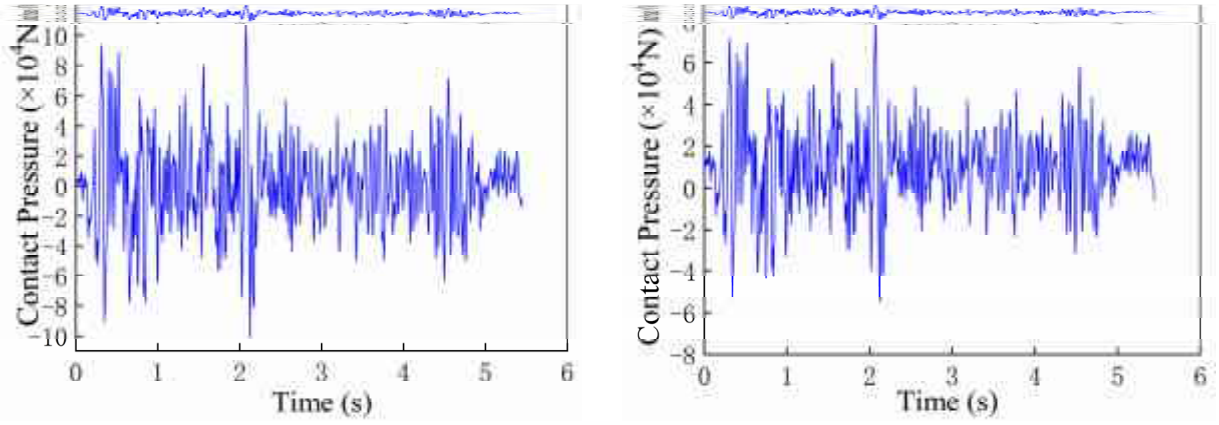

(**a**) (**b**)

Figure 17. Structural base reaction under EL-Centro wave. (**a**) X-direction base reaction force; (**b**) Z-direction base reaction force.

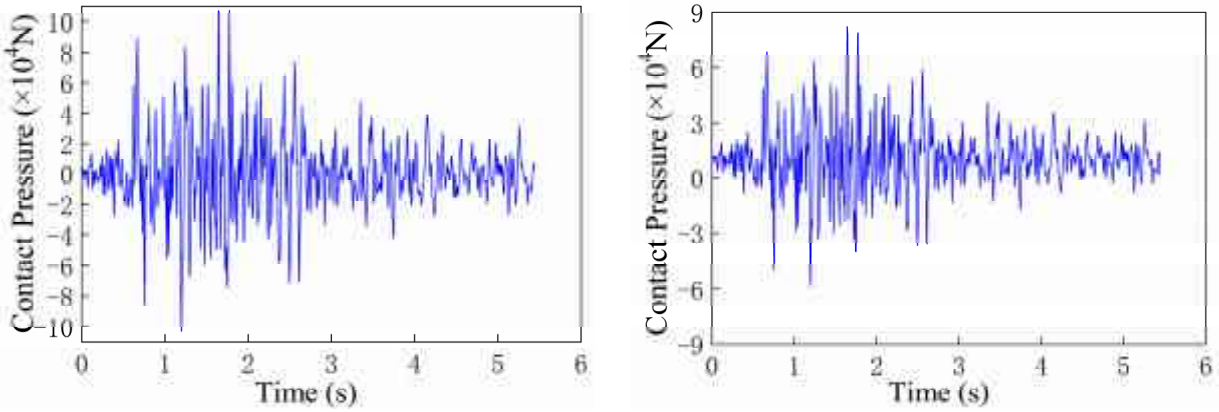

(**a**) (**b**)

Figure 18. Structural base reaction under Taft wave. (**a**) X-direction base reaction force; (**b**) Z-direction base reaction force.

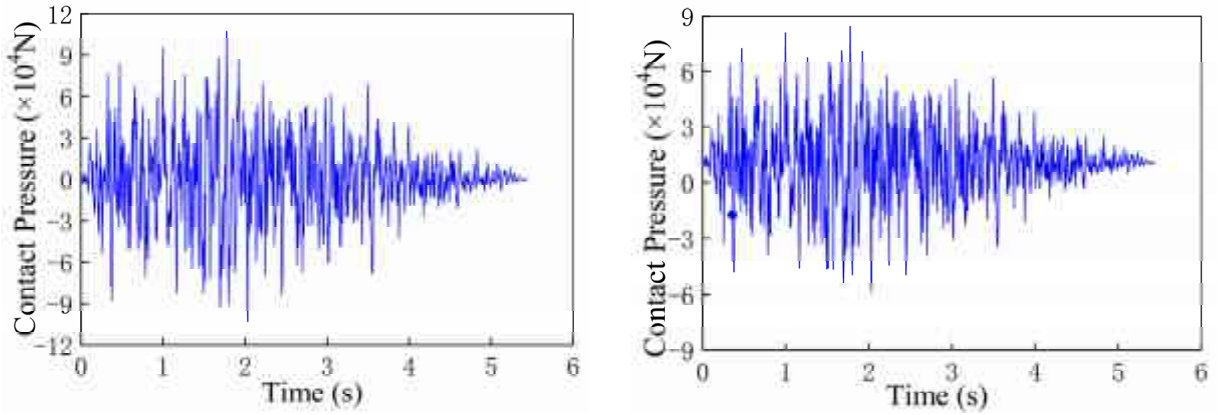

(**a**) (**b**)

Figure 19. Structural base reaction under artificial wave. (**a**) X-direction base reaction force; (**b**) Z-direction base reaction force.

Table 11. Maximum base reaction force of structure under different ground motions.

Type	Maximum Base Reaction Force in X Direction (N)	Maximum Base Reaction Force in Z Direction (N)
EL-Centro wave	106,392	79,279
Taft wave	107,338	82,189
Artificial wave	109,235	84,314
Average value	107,655	81,927.33

(2) Base reaction of three-dimensional isolation structure

The maximum base reaction force of the containment structure of a three-dimensional isolated nuclear power plant under different seismic motions is shown in Table 12.

Table 12. Maximum base reaction force and damping rate of isolated structure.

Type	Maximum Base Reaction Force in X Direction (N)	Maximum Base Reaction Force in Z Direction (N)
EL-Centro wave	80,293	201,801
Taft wave	21,244	176,438
Artificial wave	41,730	238,472
Average value	47,756	205,570

From Figures 20–22, it can be seen that under different seismic motions, the X-direction base reaction of the three-dimensional isolation structure changes very smoothly with time, indicating a decrease in shear force mutation in the horizontal direction and a decrease in the likelihood of structural shear failure. The impact of the isolation layer on the vertical reaction waveform of the structure is relatively small.

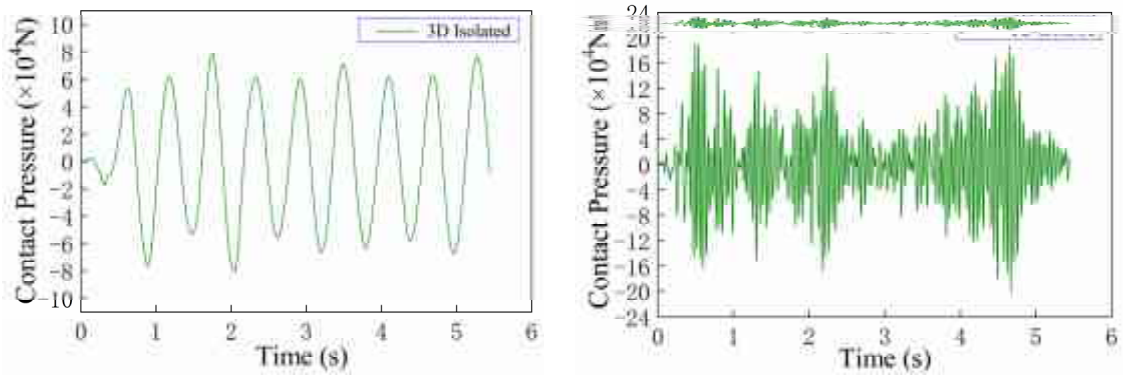

(**a**) (**b**)

Figure 20. Structural base reaction under the EL-Centro wave. (**a**) X-direction base reaction force; (**b**) Z-direction base reaction force.

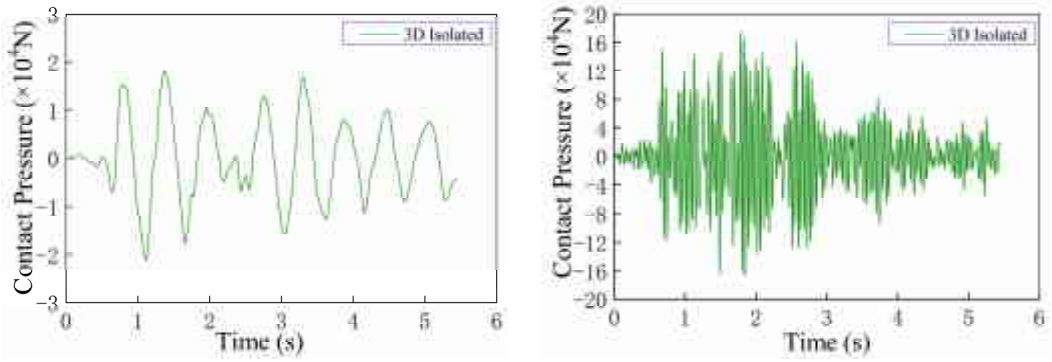

(**a**) (**b**)

Figure 21. Structural base reaction under Taft wave. (**a**) X-direction base reaction force; (**b**) Z-direction base reaction force.

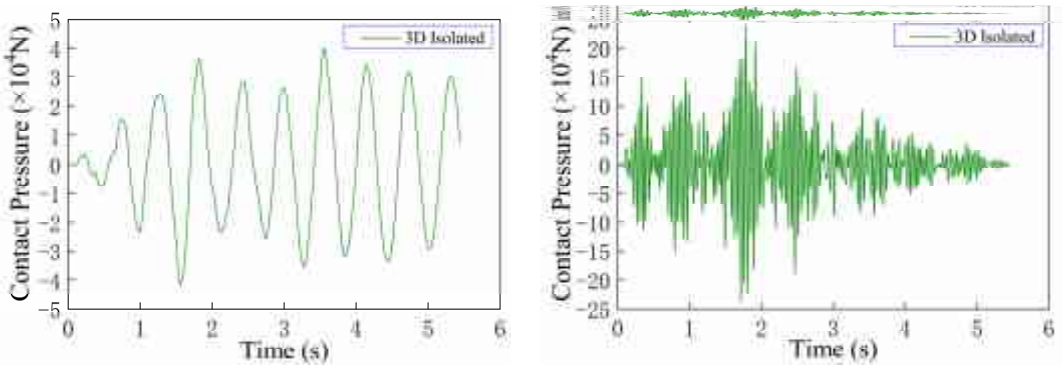

(**a**) (**b**)

Figure 22. Structural base reaction under artificial wave. (**a**) X-direction base reaction force; (**b**) Z-direction base reaction force.

3.3.3. Structural Displacement Response

(1) Acceleration response of non-isolated containment structures

Based on the time-history analysis results under different seismic motions, the X-direction displacement response of the dome and base of the nuclear power plant containment structure is obtained as shown in Figures 23a, 24a and 25a, and then the relative displacement of the dome relative to the base is obtained as shown in Figures 23b, 24b and 25b.

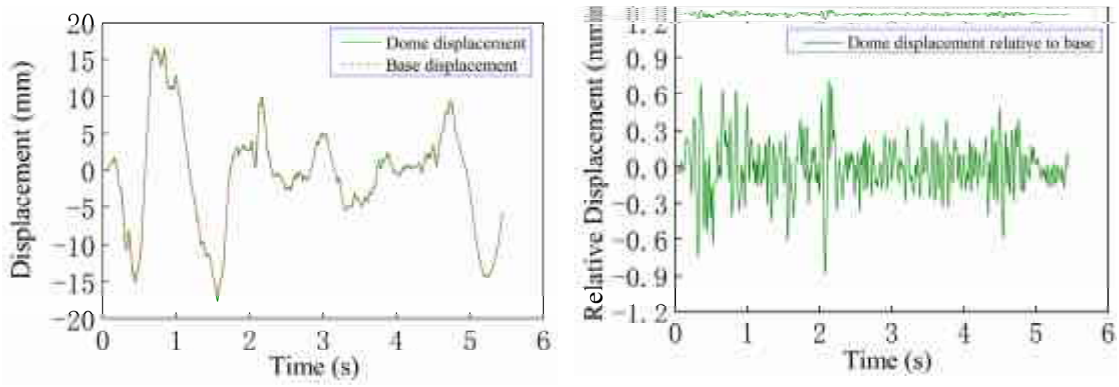

(**a**) (**b**)

Figure 23. Structural displacement response under EL-Centro wave. (**a**) Displacement; (**b**) Relative displacement.

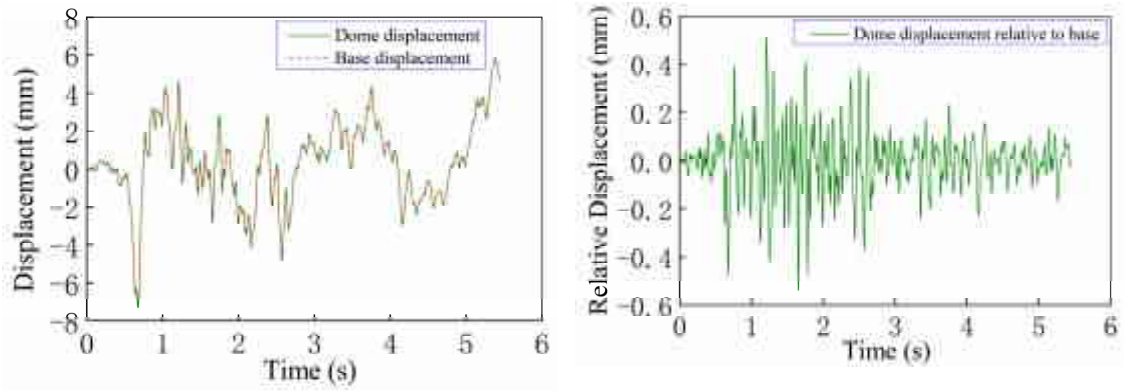

(**a**) (**b**)

Figure 24. Structural displacement response under EL-Centro wave. (**a**) Displacement; (**b**) Relative displacement.

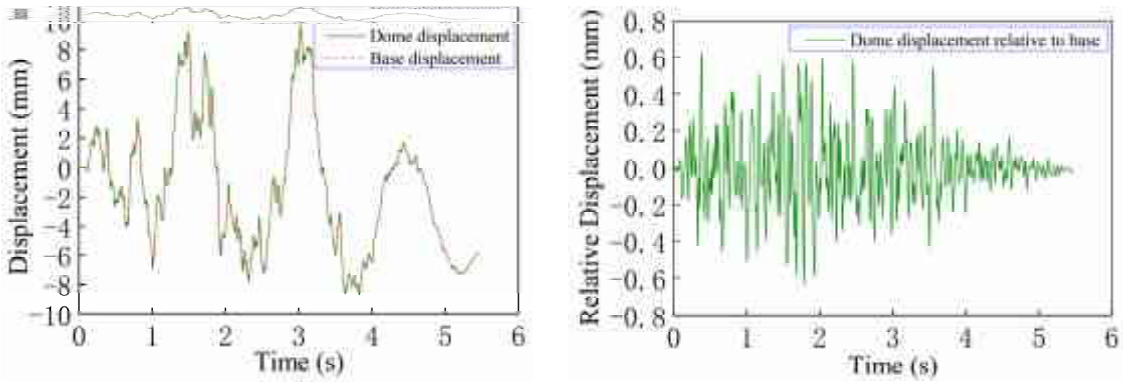

(**a**) (**b**)

Figure 25. Structural displacement response under EL-Centro wave. (**a**) Displacement; (**b**) Relative displacement.

From Figure 23, it can be seen that under the action of EL-Centro waves, the maximum displacement of the dome of the structure is 17.659 mm, and the relative displacement of the dome is the highest at 2.086 s, with a displacement value of 0.881 mm, corresponding to the prototype displacement value of 14.09 mm. As shown in Figure 24, under the action of Taft waves, the maximum displacement of the dome of the structure is 7.288 mm, and the relative displacement of the dome is the highest at 1.658 s, with a displacement value of 0.536 mm, corresponding to a prototype displacement value of 8.576 mm. As shown in Figure 25, under the action of artificial waves, the maximum displacement of the dome of the structure is 9.616 mm, and the relative displacement of the dome is the highest at 1.687 s, with a displacement value of 0.635 mm, corresponding to a prototype displacement value of 10.160 mm.

(2) Acceleration response of three-dimensional isolation structure

The displacement response of the safety shell structure of a three-dimensional isolated nuclear power plant under different seismic motions is shown in Figure 26, and the peak displacement response is shown in Table 13. The displacement time history of the isolation layer of the structure is obtained by subtracting the displacement of the input seismic motion from the bottom displacement of the upper structure, as shown in Figure 27.

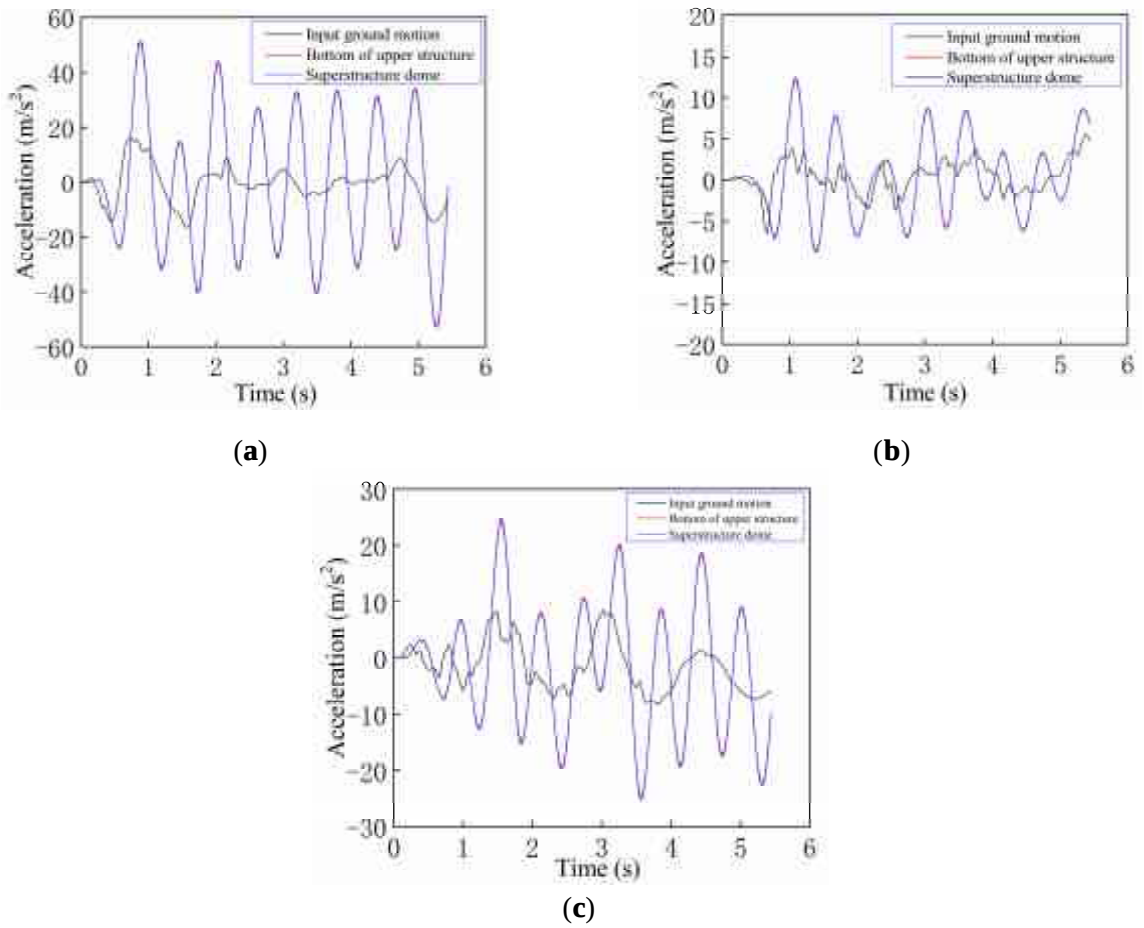

Figure 26. X-direction displacement response of containment structure under different ground motions. (**a**) EL-Centro wave; (**b**) Taft wave; (**c**) Artificial wave.

Table 13. Acceleration peaks of structural base and dome under the action of various earthquake ground motions.

Type	Peak Value at the Bottom of the Upper Structure (mm)	Peak Displacement of Upper Structure Dome (mm)	Peak Relative Displacement of Upper Structure Dome (mm)
EL-Centro wave	52.57	53.21	0.64
Taft wave	12.04	12.35	0.31
Artificial wave	24.61	25.05	0.44

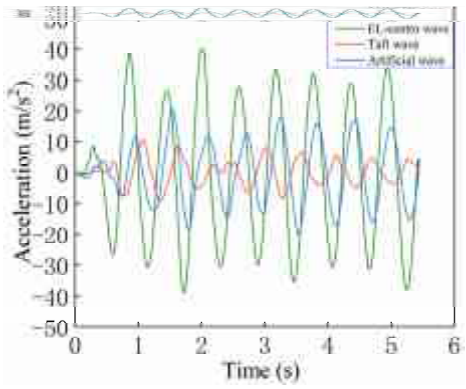

Figure 27. X-direction displacement response of structural isolation layer under different ground motions.

Based on the time-history analysis results under different seismic motions, the displacement response of the dome and isolation layer of the nuclear power plant containment structure is obtained. From Figures 26 and 27, it can be seen that the displacement response of the three-dimensional isolated nuclear safety upper structure has a significant time-delay effect on the displacement of the input seismic motion, but the displacement value is much greater than the seismic loading displacement, mainly due to the setting of the isolation layer. The displacement deformation mainly occurs in the isolation layer, and the interlayer displacement value of the upper structure is relatively small. According to the "Code for Seismic Design of Buildings", the ultimate horizontal displacement limit of isolation bearings under corresponding compressive stress should be less than the smaller value of 0.55 times their effective diameter and 3.0 times the total thickness of the rubber layer [40]. From Figure 27, it can be seen that the deformation displacement of the isolation layer is within 40 mm, which is much smaller than the design displacement of the epoxy thick rubber isolation bearing of 98 mm and the ultimate displacement value of the bearing, indicating that the deformation of the bearing is within the safe range of use.

3.4. Comparison of Time History Analysis Results between Non Isolated and Three-Dimensional Isolated Containment Structures

Based on the time-history analysis of structures under the action of EL-Central waves, Taft waves, and artificial waves, the acceleration, displacement, and other seismic responses of non-isolated and three-dimensional isolated nuclear power plant containment structures are obtained. The isolation effect is quantified by defining the damping rate, and the damping rate η is calculated according to the following equation, and the calculation results are shown in Tables 14–16.

Table 14. Damping rate of acceleration of the 3D isolated structure and non-isolated structure dome under different ground motions.

Type	Peak Acceleration in X Direction (m/s^2)			Peak Acceleration in Z Direction (m/s^2)		
	Non-Isolated	Isolation	Decreasing Amplitude Ratio (η)	Non-Isolated	Isolation	Decreasing Amplitude Ratio (η)
EL-Centro wave	7.899	4.669	40.89%	4.433	12.135	−173.74%
Taft wave	8.514	1.240	85.44%	4.958	10.788	−117.59%
Artificial wave	9.568	2.554	73.31%	5.304	14.633	−175.89%
Average value	8.660	2.821	66.55%	4.898	12.519	−155.74%

Table 15. Damping rate of maximum base reaction force of the 3D isolated structure and non-isolated structure under different ground motions.

Type	Maximum Base Reaction Force in X Direction (N)			Maximum Base Reaction Force in Z Direction (N)		
	Non-Isolated	Isolation	Decreasing Amplitude Ratio (η)	Non-Isolated	Isolation	Decreasing Amplitude Ratio (η)
EL-Centro wave	106,392	80,293	24.53%	79,279	201,801	−154.55%
Taft wave	107,338	21,244	80.21%	82,189	176,438	−114.67%
Artificial wave	109,235	41,730	61.80%	84,314	238,472	−182.84%
Average value	107,655	47,756	55.51%	81,927	205,570	−150.92%

Table 16. Damping rate of the dome displacement of the 3D isolated structure and non-isolated structure under different ground motions.

Type	Non-Isolated	Isolation	Decreasing Amplitude Ratio (η)
EL-Centro wave	17.659	53.210	201.32%
Taft wave	7.288	12.350	69.46%
Artificial wave	9.616	25.05	160.50%

Shock absorption rate η:

$$\eta = \frac{\Delta - \delta}{\delta} \times 100\% \quad (4)$$

In the equation, Δ represents the seismic response after isolation, such as displacement, acceleration, and base reaction; δ represents the seismic response before isolation.

When $\eta > 0$, the seismic response of the structure decreases, and the larger its value, the greater the isolation efficiency. When $\eta < 0$, it indicates an increase in seismic response.

From Tables 14 and 15, it can be seen that the isolation effect of isolation bearings varies under different seismic waves, with the most significant isolation effect on structures subjected to Taft waves, with a damping rate of up to 85%. Under vertical seismic action, the amplification effect of the structure on vertical acceleration and vertical reaction is the greatest under the action of EL centro and artificial waves. The results indicate that the seismic characteristics of different seismic waves have a significant impact on the isolation effect of isolation bearings. In isolation design, it is necessary to focus on analyzing the site environment of the nuclear power plant containment structure and select seismic waves that are more in line with the actual environment to make the results of structural elastic-plastic time history analysis more accurate. From Tables 15 and 16, it can be seen that under different seismic waves, the displacement response of the three-dimensional isolation nuclear power plant containment structure is much greater than that of the non-isolation structure. The interlayer displacement of the structure decreases, which is due to the significant deformation of the isolation layer and the consumption of some seismic energy, effectively reducing the interlayer displacement of the structure above the isolation layer. Research has shown that the installation of isolation layers can effectively reduce the horizontal seismic response of structures.

4. Vulnerability Analysis of Nuclear Safety Shell Structure

4.1. Basic Theory of IDA Method

Incremental dynamic analysis (IDA) is a method of selecting reasonable ground motion for building structures based on certain requirements, adjusting the amplitudes of various seismic motions, and obtaining structural responses under ground motion by loading the building structure with ground motion. We drew the relationship curve between different earthquake damage indicators DM (degree of destruction) and earthquake intensity indicators IM (intensity), which is the IDA curve. The resulting multiple curves are the "clusters" of the IDA curve [42]. The process of conducting seismic vulnerability analysis on the containment structure of a nuclear power plant using the IDA method is shown in Figure 28.

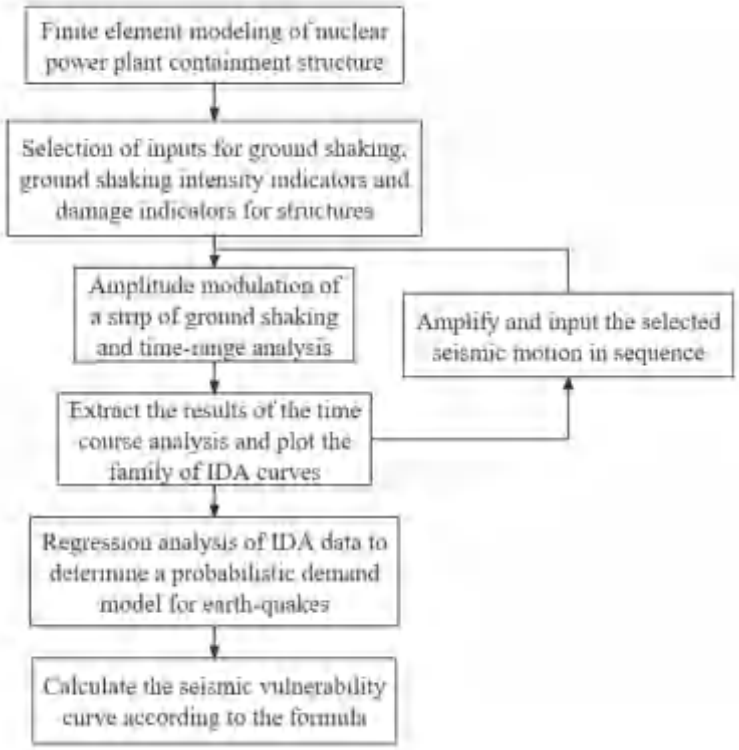

Figure 28. Flow chart of seismic vulnerability analysis.

4.1.1. Ground Motion Selection

The uncertainty of seismic motion will cause discreteness of the structural seismic response. According to the selection principle, the standard design response spectrum of nuclear safety structures should be as close as possible to the average response spectrum of selected seismic motion records, with an earthquake level distribution of 5.0–7.5. This article selects 12 natural earthquake motion records from the latest earthquake motion record sharing database of the Pacific Earthquake Engineering Research Center (PEER) in the United States for analysis, as shown in Table 17. The corresponding seismic response spectrum and standard design response spectrum are shown in Figure 29.

Table 17. Records of 12 natural ground motions.

Serial Number	Ground Motion Name	Occurrence Time	Location of Measuring Points	Strength Grade	PGA/g
1	Helena Montana-01	1935	Carroll College	6.00	0.646
2	Northwest Calif-01	1938	Ferndale City Hall	6.95	0.486
3	Northwest Calif-02	1941	Ferndale City Hall	6.60	0.245
4	Borrego	1942	El Centro Array #9	6.50	0.237
5	Kern County	1952	LA—Hollywood Stor FF	7.36	0.224
6	Southern Calif	1952	San Luis Obispo	6.00	0.208
7	El Alamo	1956	El Centro Array #9	6.80	0.398
8	Hollister-01	1961	Hollister City Hall	5.60	0.277
9	Lytle Creek	1970	Wrightwood-6074 Park Dr	5.33	0.581
10	San Fernando	1971	2516 Via Tejon PV	6.61	0.142
11	Point Mugu	1973	Port Hueneme	5.65	0.324
12	Hollister-03	1974	Hollister City Hall	5.14	0.623

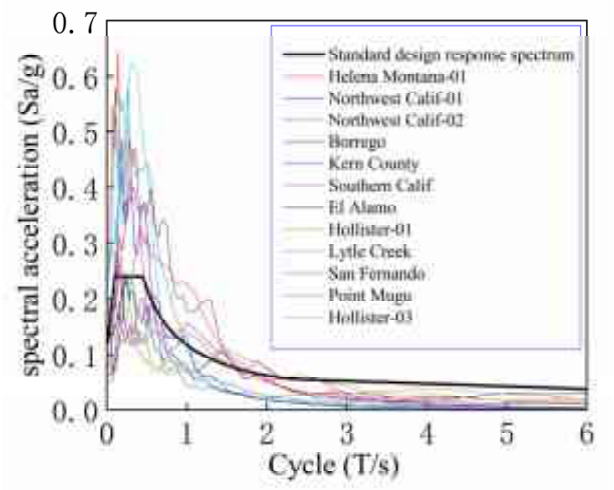

Figure 29. Response spectrum of ground motion and standard design response spectrum.

4.1.2. Selection of Ground Vibration Intensity Indicators

Spectral acceleration (Sa), peak velocity (PGD), peak acceleration (PGA), and other indicators are usually used as seismic intensity indicators for structural vulnerability analysis, and the selection of these indicators has a significant impact on structural analysis. Mackie and Stojadinovi analyzed the probability results in a logarithmic coordinate system [43] and found that using PGA and PGV as strength indicators has good applicability to IM; The Seismic Design Code for Nuclear Power Plants considers PGA as the seismic intensity index and seismic fortification standard for nuclear power plants [41]. Padgett et al. used different seismic intensity indicators to evaluate and analyze their specificity, effectiveness, and computability. The study found that PGA as the intensity indicator was the optimal choice [44]. Therefore, PGA is selected as the seismic intensity index for IDA vulnerability analysis.

4.1.3. Selection of Structural Failure Indicators

The damage measure (DM) of a structure refers to the variable that changes with the variation of the vibration intensity index of the structure. Common DM indicators include the following: maximum inter-story displacement angle, maximum vertex displacement, maximum floor ductility, maximum base shear force, etc. The containment structure of a nuclear power plant serves as the last barrier to prevent nuclear leakage. Once the structure cracks, it is considered to have been damaged. The failure mode of this structure is usually the weak position in contact between the cylinder and the bottom plate, which is prone to shear loading failure under strong earthquakes. The displacement of the structural vertices relative to the bottom plate can effectively reflect the failure state of the structure; that is, the maximum interlayer displacement of the vertices is the cracking displacement of the safety shell structure. The magnitude of the crack displacement value of the nuclear power plant containment structure can be determined using the pushover analysis method. It is subjected to unidirectional pushover using a uniform loading mode, as shown in Figure 30a, and its pushover curve is obtained as shown in Figure 30b. The displacement value for determining the damage index of the containment structure is 1.126 mm. According to the similarity relationship in Table 2, the damage displacement value of the original structure is 18.016 mm. The following calculation results are given based on the response values of the original structure.

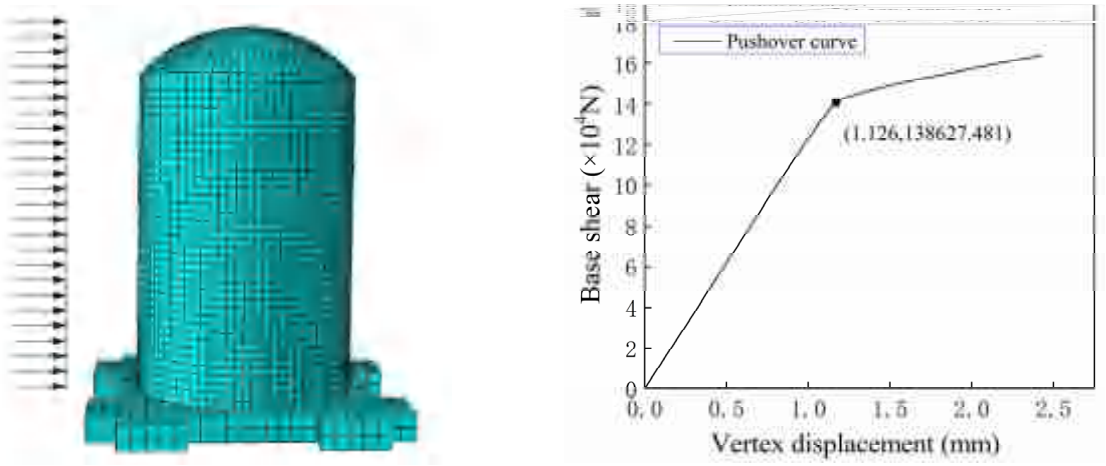

(**a**) (**b**)

Figure 30. Loading mode and curve of pushover analysis. (**a**) Uniform loading mode; (**b**) Pushover curve.

4.1.4. IDA Curve Drawing

We adjusted the amplitude of the selected seismic motion with different intensities, with an initial PGA of 0.2 g and increments of 0.2 g per step. We used 10 amplitudes, with a maximum PGA of 2.0 g. Then we adjusted the seismic intensity based on the principle of similarity, performed nonlinear time history analysis on the containment structure, obtained the horizontal displacement of the structural vertex corresponding to PGA, and then established a DM-IM Cartesian coordinate system and drew a smooth IDA curve (as shown in Figure 31).

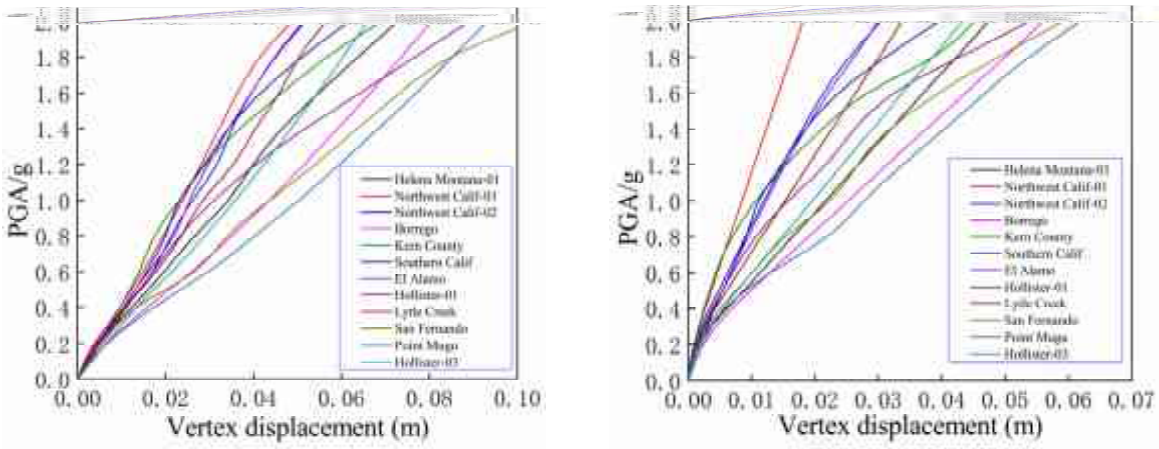

(**a**) (**b**)

Figure 31. IDA curve cluster of the non-isolated and 3D isolated nuclear containment structure. (**a**) Non-isolated structure; (**b**) Three-dimensional seismic isolation structures.

From Figure 31, it can be seen that the structural IDA curves obtained under different seismic actions are different. To reduce the dispersion problem of structural response values under different seismic actions, statistical regression can be performed by selecting reasonable percentile values. Typically, three IDA curves with probability percentiles of 16%, 50%, and 84% are taken, as shown in Figure 32.

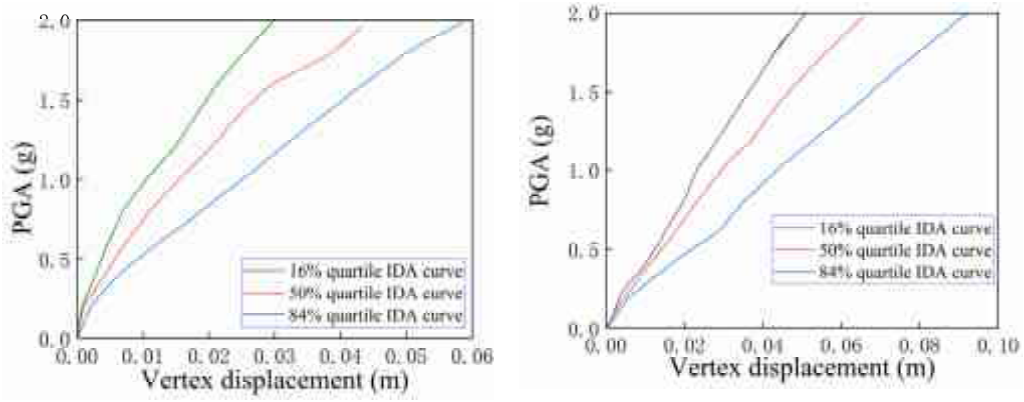

(**a**) (**b**)

Figure 32. Fractional IDA curve of the non-isolated and 3D isolated nuclear containment structure. (**a**) Non-isolated structure; (**b**) Three-dimensional seismic isolation structures.

By selecting percentile values, the IDA curve is determined to be more representative, reflecting the seismic intensity of the structure at the damage location. From Figure 32, it can be seen that the percentile values of the non-isolated nuclear power plant containment structure are 16%, 50%, and 84% IDA curves, which correspond to the seismic intensity of 0.4 g, 0.6 g, and 0.75 g, respectively, when the structure is damaged. The percentile values of the non-isolated nuclear power plant containment structure are 16%, 50%, and 84% IDA curves, which correspond to the seismic intensity of 0.6 g, 0.8 g, and 1.22 g when the structure is damaged, respectively. The results indicate that in order to achieve the structural damage value, the seismic intensity required for isolated structures is greater.

4.2. Establishment of Seismic Vulnerability Curve

4.2.1. Establishment of Earthquake Probability Demand Model

We performed incremental dynamic analysis on non-isolated and isolated containment structures, taking the logarithm of the seismic intensity index *IM* and structural damage index DM. According to Equation (5), we established a Cartesian coordinate system with ln (*PGA*) as the abscissa and ln(*y*) as the ordinate, and performed linear regression analysis (as shown in Figure 33) to obtain the seismic probability demand model for non-isolated and three-dimensional isolated nuclear power plant containment structures.

$$\ln D' = a + b\ln(IM) \tag{5}$$

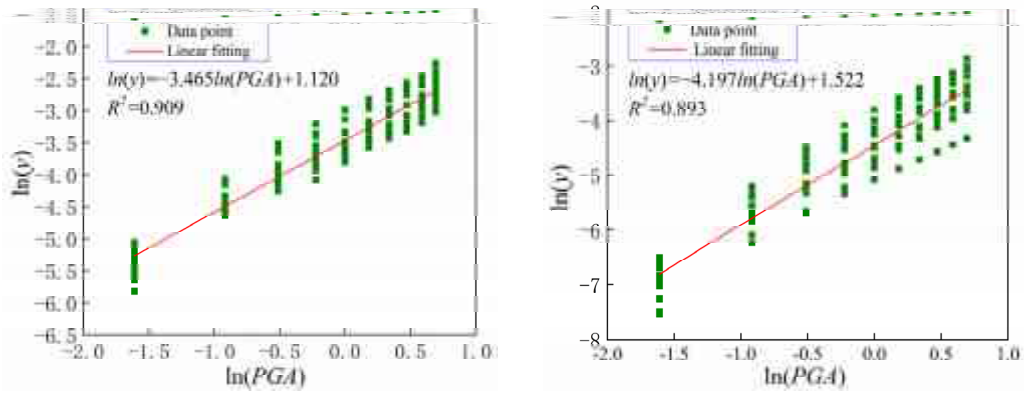

(**a**) (**b**)

Figure 33. Seismic probability demand model for nuclear containment structure. (**a**) Non isolated structure; (**b**) Three-dimensional seismic isolation structures.

In the equation: The median value of seismic demand parameters; IM—Ground motion intensity index. *a b*—Regression coefficient, $a = \ln \alpha$, $B = \beta$. The IDA data for incremental dynamic analysis of the containment structure of nuclear power plants were analyzed using linear regression to obtain the corresponding values of a and b.

According to Equation (5), the mathematical expression for the seismic probability demand model of the containment structure of non-isolated nuclear power plants is obtained:

$$\ln(y) = -3.465 \ln(PGA) + 1.120 \tag{6}$$

In the equation, if $a = \ln \alpha = -3.465$, then $\alpha = 0.0316$ and $b = \beta = 1.120$.

Similarly, the mathematical expression for the seismic probability demand model of the containment structure of a three-dimensional isolated nuclear power plant is:

$$\ln(y) = -4.197 \ln(PGA) + 1.522 \tag{7}$$

In the equation, if $a = \ln \alpha = -4.197$, then $\alpha = 0.0152$ and $b = \beta = 1.522$.

4.2.2. Drawing of Seismic Vulnerability Curve

The formula for calculating the probability of structural failure with the maximum peak acceleration *PGA* as the independent variable is:

$$P_f = \Phi\left\{ \frac{\ln\left[\alpha (PGA)^{\beta} / C'\right]}{\sqrt{\beta_c^2 + \beta_d^2}} \right\} \tag{8}$$

In the formula, $\Phi(X)$ is the standard normal distribution function, and C' is determined by the pushover analysis results of the nuclear power plant containment structure; According to the High Standard Seismic Design Specification for Structural Vulnerability Curve Parameters (HAZUS99) [45], when *PGA* is taken as *IM*, $\sqrt{\beta_c^2 + \beta_d^2}$ can be taken as 0.5. The probability of the structure reaching the set damage index value under earthquake action of different intensities is:

$$P_f = \Phi\left\{ \frac{\ln\left[0.0316 \times (PGA)^{1.120} / 0.018\right]}{0.5} \right\} \tag{9}$$

$$P_f = \Phi\left\{ \frac{\ln\left[0.0152 \times (PGA)^{1.522} / 0.018\right]}{0.5} \right\} \tag{10}$$

Using PGA as the horizontal axis and P_f as the vertical axis, we drew the relationship curve between PGA and P_f, which is the seismic vulnerability curve of the nuclear power plant containment structure, as shown in Figure 34.

From Figure 34, it can be seen that when the seismic intensity is below 0.2 g, the failure probability of non-isolated nuclear safety structures is approximately 0; The probability of failure of the containment structure of a three-dimensional isolated nuclear power plant is approximately 0 when the seismic motion is less than 0.4 g. This indicates that under the action of small earthquakes, the two types of nuclear safety structures almost do not undergo damage, which is determined by the structural characteristics and the relatively high stiffness; Under rare earthquakes, the probability of failure of the safety shell structure of non-isolated nuclear power plants reaches 15%, and the safety shell structure of three-dimensional isolated nuclear power plants is just beginning to be damage.

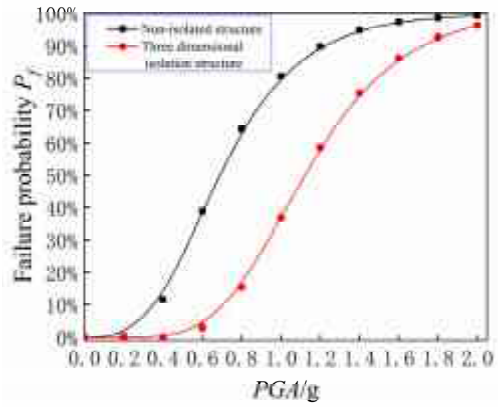

Figure 34. Seismic fragility curve of nuclear containment structure.

From the overall seismic vulnerability curve, as the seismic intensity gradually increases, the overall trend of the failure probability of the two types of structures remains consistent. The overall growth rate of the failure probability is from slow to urgent and then to slow. The failure probability of non-isolated nuclear power plant containment structures is basically above that of isolated structures, and the probability difference between the two first increases and then decreases. The results indicate that under the same seismic intensity, the three-dimensional isolation nuclear power plant containment structure has a large seismic margin, and the installation of isolation layers effectively enhances the seismic performance of the structure.

5. Conclusions and Discussion

5.1. Conclusions

This article presents the design and performance study of thick rubber isolation bearings for three-dimensional isolation of nuclear power plant containment structures. We establish finite element models of non-isolated and three-dimensional isolated nuclear power plant containment structures, and study the isolation effect of isolation bearings in the structure. Finally, through the theory of structural seismic vulnerability analysis, the seismic margin of the containment structure of isolated nuclear power plants is compared and analyzed. The conclusion is as follows:

By comparing the modal analysis results of non-isolated and three-dimensional isolated nuclear power plant containment structures, it was found that compared to non-isolated structures, the natural vibration period of three-dimensional isolated structures is longer, and the natural vibration period of three-dimensional isolated structures is 0.558 s. Based on the similarity relationship, the natural vibration period of the prototype of the three-dimensional isolated nuclear power plant containment structure is 3.077 s.

By conducting a time history analysis of a seismic wave intensity of 0.608 on the safety shell structures of non-isolated and three-dimensional isolated nuclear power plants, and comparing the acceleration, base reaction, displacement, and other responses of the structures, it is shown that under the action of EL-Centro waves, Taft waves, and artificial waves, the isolation bearings exhibit different seismic reduction effects, with seismic reduction rates reaching 41%, 85%, and 73%, respectively. The results show that the seismic characteristics of different seismic waves have a significant impact on the isolation effect of the isolation bearings, among which the isolation effect on structures subjected to Taft waves is the most significant; Under the action of three types of seismic waves, the displacement and seismic reduction rates of the isolation structure reached 201%, 69%, and 160%, causing the isolation layer to consume most of the energy, reducing the inter-story displacement of the structure above the isolation layer and effectively reducing the horizontal seismic response of the structure with three-dimensional isolation bearings.

This study adopts a new type of epoxy plate thick layer rubber isolation bearing, with a hole diameter of 0, a rubber shear modulus of 1.0 MPa, a rubber layer to stiffener

thickness ratio of 1.5, and 9 rubber layers. By comparison, it was found that the stability of the epoxy thick layer rubber isolation bearings without holes was significantly improved compared to those with holes, and the magnitude of concentrated stress was significantly reduced. When the local seismic intensity is below 0.2 g, the failure probability of non-isolated nuclear safety structures is approximately 0, and the safety shell structure of a three-dimensional isolated nuclear power plant does not suffer damage when the seismic motion is less than 0.4 g. The increase in local vibration intensity leads to an overall trend of both failure probabilities from slow to rapid and then to slow. Under the same seismic intensity, the safety shell structure of a three-dimensional isolated nuclear power plant has a large seismic margin, and the setting of isolation layers effectively enhances the seismic performance of the structure.

5.2. Discussion

There are still shortcomings in the research on the safety structure of three-dimensional isolated nuclear power plants, and further research is needed:

There are still shortcomings in the elastic-plastic time history analysis and structural vulnerability analysis of the safety structure of a three-dimensional isolated nuclear power plant. This article did not consider the actual coupled biaxial hysteresis behavior exhibited by the elastic isolation device. It is necessary to simulate the biaxial horizontal coupling behavior of the equipment used in future research.

The vulnerability analysis of the safety shell structure in nuclear power plants does not consider damage to the internal structure, which has certain limitations.

Author Contributions: Conceptualization, Q.P. and Z.X.; Methodology, Q.P., J.Z. and Z.X.; Software, X.C. and Y.Z.; Validation, Q.P., Y.H. and Z.X.; Formal analysis, Q.P. and Z.X.; Investigation, X.C. and Y.Z.; Data curation, Y.Z., J.Z. and Y.H.; Writing—original draft preparation, Z.X., X.C. and Y.Z.; Writing—review and editing, Q.P.; Supervision, Q.P., X.C. and Z.X.; Project administration, Z.X. and Q.P.; Formal analysis, Y.Z. and Y.H.; Funding acquisition, Z.X. and J.Z.; All authors have read and agreed to the published version of the manuscript.

Funding: This research was funded by the Guangdong Province Youth Innovation Talent Project for Ordinary Universities, Research on Mechanical Characteristics of Steel Strand Rope Broken Wire Damage Based on Fine Finite Element Model (grant no. 2019KQNCX086), Guangdong Provincial Basic and Applied Basic Research Fund Natural Science Foundation Project, Research on Damage and Degradation Mechanism and Seismic Performance Evaluation of Stay Cables under Complex Factor Coupling (grant no. 2021A1515010573), the University Characteristic Innovation Project of Guangdong Province Education Foundation (grant no. 2019KTSCX102), Dalian University Research Platform Project (202301ZD01).

Data Availability Statement: The data used to support nuclear power plant research are confidential and cannot be disclosed. If data is required, they must be obtained from the corresponding author as required.

Conflicts of Interest: The authors declare no conflicts of interest.

References

1. Zou, X.; Yang, W.; Liu, P.; Wang, M. Shaking table tests and numerical study of a sliding isolation bearing for the seismic protection of museum artifacts. *J. Build. Eng.* **2023**, *65*, 105725. [CrossRef]
2. Nie, G.B.; Zhang, C.X.; Wang, Z.Y.; Xu, W.D.; Shi, Y.J. Shaking table test of space double-layer cylindrical reticulated shell with three-dimensional isolation bearing. *J. Constr. Steel Res.* **2022**, *189*, 107107. [CrossRef]
3. Park, K.G.; Chung, M.J.; Lee, D.W. Earthquake response an analysis for seismic isolation system of single layer lattice domes with 300m span. *J. Korean Assoc. Spat. Struct.* **2018**, *18*, 105–116. [CrossRef]
4. Jamalvandi, M.; Amiri, M. Influence of Seismic Isolation Systems on Behavior of Fluid inside Thin-walled Steel Tanks. *Jordan J. Civ. Eng.* **2021**, *15*, 534.
5. Lu, Y.; Song, J.; Xiong, F.; Lu, Y.; Song, J.; Xiong, F.; Dai, K.; Zhou, G.; Wei, M.; Zhang, S. Simplified procedures for seismic design verification and evaluation of lead rubber bearing base-isolated buildings based on free-vibration response. *Struct. Des. Tall Spec. Build.* **2020**, *29*, e1751. [CrossRef]

6. Cao, S.; Ozbulut, O.E.; Wu, S.; Sun, Z.; Deng, J. Multi-level SMA/lead rubber bearing isolation system for seismic protection of bridges. *Smart Mater. Struct.* **2020**, *29*, 055045. [CrossRef]
7. Liu, Q.; Guo, Z.; Zhu, S.; Wang, C.; Ren, X.; Wu, X. Performance-Based Seismic Design of Hybrid Isolation Systems with Gap-Tunable BRBs for Bearing-Supported Bridges. *Symmetry* **2022**, *14*, 1373. [CrossRef]
8. Wang, T.; Wang, F.; Dinglu, T.; Hougang, L. Shaking table teste on base-isolated nuclear power plant. *J. Eng. Mech.* **2014**, *31*, 62–68+84. [CrossRef]
9. Suduo, X.; Mingyue, S.; Xiongyan, L.; Shuanzhu, L.; Fuyun, H.; Yi, L. Shaking table test and numerical simulation of an isolated cylindrical latticed shell under multiple-support excitations. *Earthq. Eng. Eng. Vib.* **2019**, *18*, 611–630. [CrossRef]
10. Nikfar, F.; Konstantinidis, D. Experimental study on the seismic response of equipment on wheels and casters in base-isolated hospitals. *J. Struct. Eng.* **2019**, *145*, 04019001. [CrossRef]
11. Koo, G.H.; Shin, T.M.; Ma, S.J. Shaking table tests of lead inserted small-sized laminated rubber bearing for nuclear component seismic isolation. *Appl. Sci.* **2021**, *11*, 4431. [CrossRef]
12. Chen, Y.; Sun, H.; Feng, Z. Study on seismic isolation of long span double deck steel truss continuous girder bridge. *Appl. Sci.* **2022**, *12*, 2567. [CrossRef]
13. Wei, B.; He, W.; Jiang, L.; Wang, Z. Influence of pier height on the effectiveness of seismic isolation of friction pendulum bearing for single-track railway bridges. *Smart Struct. Syst. Int. J.* **2021**, *28*, 213–228. [CrossRef]
14. He, W.; Jiang, L.; Wei, B.; Wang, Z. The influence of pier height on the seismic isolation effectiveness of friction pendulum bearing for Double-Track railway bridges. In *Structures*; Elsevier: Amsterdam, The Netherlands, 2020; Volume 28, pp. 1870–1884. [CrossRef]
15. Nie, G.; Liu, K. Experimental studies of single-layer reticulated domes with isolated supports. *Shock. Vib.* **2018**, *2018*, 6041878. [CrossRef]
16. Frano, R.L.; Forasassi, G. Isolation systems influence in the seismic loading propagation analysis applied to an innovative near term reactor. *Nucl. Eng. Des.* **2010**, *240*, 3539–3549. [CrossRef]
17. Sun, F.; Pan, R.; Wang, W. Simulation Analysis of Seismic Isolation Dynamic R esponse Lawson Concrete Containment in Nuclear Power Plants. *Eng. Seism. Resist. Reinf. Renov.* **2014**, *36*, 27–30.
18. Zhao, C.F. Study on Dynamic Response and Measures of Seismic Reduction and Anti-explosion of Nuclear Island Subjected to Strong Earthquakes and Blast Loads. Ph.D. Thesis, Dalian University of Technology, Dalian, China, 2014.
19. Zhao, C.F.; Chen, J.Y. The influence of basic isolation system on seismic resistance of nuclear power plant containment. *Explos. Shock. Waves* **2014**, *34*, 615–621.
20. Fan, S.K.; Tan, P.; Liu, D.W. Research on seismic isolation of nuclear power plant structures. *J. Disaster Prev. Mitig. Eng.* **2015**, *35*, 685–690. [CrossRef]
21. Tan, P.; Fan, S.K.; Xu, K. Research on seismic isolation of nuclear power plant reactor building. *J. Guangzhou Univ. (Nat. Sci. Ed.)* **2014**, *13*, 28–35.
22. Ashiquzzaman, M.; Hong, K.-J. Simplified Model of Soil-Structure Interaction for Seismically Isolated Containment Buildings in Nuclear Power Plant. In *Structures*; Elsevier: Amsterdam, The Netherlands, 2017; Volume 10, pp. 209–218. ISSN 2352-0124. [CrossRef]
23. Zhao, Z.; Wang, Y.; Hu, X.; Weng, D. Seismic performance upgrading of containment structures using a negative-stiffness amplification system. *Eng. Struct.* **2022**, *262*, 114394. [CrossRef]
24. Han, G.; Wu, Y.; Hou, G.; Yue, Z. Optimal design of earthquake-resistant containment for FPS-Isolated nuclear power plants with electromagnetic tuned liquid column damper inerter. *J. Mech. Sci. Technol.* **2024**, *38*, 579–594. [CrossRef]
25. Wei, L.S.; Zhang, Y.S.; Kong, D.R. Study on Three-dimensional Seismic Isolation of Nuclear Island. *South China J. Seismol.* **2015**, *35*, 37–42.
26. Nie, G.B.; Zhang, C.X.; Wang, Z.Y.; Shi, Y.J. Shaking Table Study of the Three-Dimensional Isolation of a Cylindrical Reticulated Shell. *Int. J. Steel Struct.* **2022**, *22*, 502–513. [CrossRef]
27. Nie, G.B.; Li, D.F.; Zhi, X.D.; Chen, Q.; Wang, F.Y. Three-dimensional seismic isolation study of single-layer reticulated domes by parameter analysis. *Int. J. Steel Struct.* **2021**, *21*, 1953–1965. [CrossRef]
28. Zhuang, P.; Zhao, W.; Yang, T.Y. Seismic protection of a single-layer spherical lattice shell structure using a separated three-dimensional isolation system. *Soil Dyn. Earthq. Eng.* **2023**, *172*, 108026. [CrossRef]
29. Li, X.; Liang, S.; Xue, S. Experimental research on anti-uplift three-dimensional seismic isolation bearing. In Proceedings of the IASS Annual Symposia, Barcelona, Spain, 7–10 October 2019; International Association for Shell and Spatial Structures (IASS): Madrid, Spain, 2019; pp. 1–8.
30. Zhang, C.X.; Nie, G.B.; Dai, J.W.; Liu, K.; Zhi, X.D.; Ma, H.H. Seismic isolation research on a double-layer lattice structure using shaking table tests. *Int. J. Steel Struct.* **2019**, *19*, 1237–1248. [CrossRef]
31. Liang, N.; Zhi, X.; Nie, G.; Fan, F. Experiment and Analysis of Seismically Isolated Single-Layer Cylindrical Reticulated Shell Structure. *J. Struct. Eng.* **2022**, *148*, 04022009. [CrossRef]
32. De Domenico, D.; Losanno, D.; Vaiana, N. Experimental tests and numerical modeling of full-scale unbonded fiber reinforced elastomeric isolators (UFREIs) under bidirectional excitation. *Eng. Struct.* **2023**, *274*, 115118. [CrossRef]
33. Abe, M.; Yoshida, J.; Fujino, Y. Multiaxial behaviors of laminated rubber bearings and their modeling. II: Modeling. *J. Struct. Eng.* **2004**, *130*, 1133–1144. [CrossRef]

34. Su, J.Y. *Introduction to Seismically Insulated Buildings*; Metallurgical Industry Press: Beijing, China, 2012. (In Chinese)
35. Ma, D.P. Earthquake Response Analysis of Lng Storage Tank with Seismic Isolation. Ph.D. Thesis, Harbin Institute of Technology, Harbin, China, 2007. (In Chinese)
36. Liu, L. Numerical Simulation Research on Shaking Table Test of Nuclear Containment Vessel. Ph.D. Thesis, Harbin Institute of Technology, Harbin, China, 2009. (In Chinese)
37. Liu, M. The Comparative Study on Aseismic Performace of Nuclear Containment's General Structure and Base-Isolated Structure. Ph.D. Thesis, Harbin Institute of Technology, Harbin, China, 2013. (In Chinese)
38. Wang, F. Theoretical and Experimental Study on Base-Isolated Nuclear Power Plant. Ph.D. Thesis, Institute of Engineering Mechanics, China Earthquake Administration, Harbin, China, 2013. (In Chinese)
39. Qi, W. *ABAQUS 6.14 Super Learning Handbook*; The People's Posts and Telecommunications Press: Beijing, China, 2016. (In Chinese)
40. *GB50011-2010*; Code for Seismic Design of Buildings. China Architecture & Building Press: Beijing, China, 2016. (In Chinese)
41. *GB 50267-2019*; Standard for Seismic Design of Nuclear Power Plants. China Architecture & Building Press: Beijing, China, 2019. (In Chinese)
42. Zhi, P.Y. Seismic Margin Analysis of Nuclear Containment Structure Based on Reliability Theory. Ph.D. Thesis, Heilongjiang University of Science and Technology, Harbin, China, 2018. (In Chinese)
43. Mackie, K.R.; Stojadinović, B. *Fragility Basis for California Highway Overpass Bridge Seismic Decision Making*; Pacific Earthquake Engineering Research Center, College of Engineering, University of California: Berkeley, CA, USA, 2005.
44. Padgett, J.E.; Nielson, B.G.; Desroches, R. Selection of optimal intensity measures in probabilistic seismic demand models of highway bridge portfolios. *Earthq. Eng. Struct. Dyn.* **2008**, *37*, 711–725. [CrossRef]
45. Xu, L.H.; Shan, X.; Li, Z.X. Vulnerability analysis and optimization design for steel framestructure under strong earthquakes. *Eng. Mech.* **2013**, *30*, 175–179. (In Chinese)